An Error Propagation Model of a Heliostat

by
Xiao ZHENG

Thesis presented in partial fulfilment of the requirements for the degree of Master of Engineering (Mechatronic) in the Faculty of Engineering at Stellenbosch University

Supervisor: Dr. Willie Smit
Co-supervisor: Prof. Kristiaan Schreve

March 2017

Declaration

By submitting this thesis electronically, I declare that the entirety of the work contained therein is my own, original work, that I am the sole author thereof (save to the extent explicitly otherwise stated), that reproduction and publication thereof by Stellenbosch University will not infringe any third party rights and that I have not previously in its entirety or in part submitted it for obtaining any qualification.

Date: March 2017

Abstract

An Error Propagation Model of a Heliostat

Zheng Xiao

Department of Mechanical and Mechatronic Engineering,
University of Stellenbosch,
Private Bag X1, Matieland 7602, South Africa.

Thesis: MEng (Mech)

March 2017

Concentrating solar power plants are becoming a viable option to produce renewable electricity. However, these plants are still a relative new technology and are more expensive than traditional coal fired power plants. Currently many research groups are looking into ways that will make these plants more efficient and cheaper.

A concentrating solar power plant type that seems promising at the moment, is the central tower with receiver type. This type of plant consists of a field of thousands of mirrors or heliostats that reflect solar rays onto the central receiver. The heliostat field is expensive and a lot of effort is going into reducing its cost.

Heliostats have to reflect solar rays onto the central receiver with great accuracy. Most heliostats are controlled in an open-loop fashion, which requires a very accurate and calibrated model of each heliostat. There is a need to better understand the relationship between calibration errors and tracking accuracy. Such an understanding can help engineers to focus on those aspects of the heliostat that most affect the tracking accuracy.

This work uses a common heliostat model that consists of eight parameters. It applies the error propagation law to the model in order to derive an error model of a heliostat. With the error model, it is possible analyses the relationship between calibration errors and tracking accuracy.

Uittreksel

'N Fout Voortplanting Model van 'n heliostaat

Zheng Xiao

Departement Meganiese en Megatroniese Ingenieurswese,
Universiteit van Stellenbosch,
Privaatsak X1, Matieland 7602, Suid Afrika.

Tesis: MIng (Meg)

Maart 2017

Gekonsentreerde sonkrag aanlegte is besig om 'n lewensvatbare opsie te word om hernubare elektrisiteit op te wek. Tog is hierdie aanlegte nog steeds 'n relatief nuwe tegnologie en is duurder as tradisionele steenkoolkragstasies. Tans is daar verskeie navorsingsgroepe wat maniere ondersoek om hierdie aanlegte meer doeltreffend en goedkoper te maak.

'n Gekonsentreerde sonkrag aanleg tipe wat op die oomblik belowend is, is die sentrale toring met ontvanger tipe. Hierdie tipe aanleg bestaan ??uit 'n veld van duisende spieëls of heliostate wat son strale na die sentrale ontvanger weerkaars. Die heliostaat veld is duur en 'n baie moeite gaan daarin om dit goedkoper te maak.

Heliostate moet son strale na die sentrale ontvanger weerkaats met hoë akkuraatheid. Die meeste heliostate word beheer in 'n oop-lus, wat dit nodig maak vir 'n baie akkurate en gekalibreer model van elke heliostaat. Daar is 'n behoefte om beter te verstaan wat ??die verhouding is tussen kalibrasie foute en volgingsakkuraatheid. 'n Beter begrip hiervan kan ingenieurs help om te fokus op daardie aspekte van die heliostaat wat die meeste invloed het op die volgingsakkuraatheid.

Hierdie werk maak gebruik van 'n algemene heliostaat model wat bestaan uit agt parameters. Dit pas die fout voortplantingswet op die model toe om 'n foutmodel van 'n heliostaat af te lei. Met die foutmodel, is dit moontlik om die verhouding tussen kalibrasie foute en volgingsakkuraatheid te analiseer.

Acknowledgements

I would like to express my sincere gratitude to the following people and organisations:

My sincere and hearty thanks and appreciations go firstly to my supervisor, Dr. Willie Smit, whose suggestions and encouragement have given me much insight into these research studies. It has been a great privilege and joy to study under his guidance and supervision. Furthermore, He has walked me through all the stages of the writing of this thesis. Without his patient and consistent instruction, this thesis could not have reached its present form.

Prof Kristiaan Schreve, my co-supervisor, for his patients and valuable comments on error propagation law.

The Solar Thermal Energy Research Group for they knowledge supports and for bring me to have a better view on different types of solar plants.

Dedications

I would like to dedicate this dissertation to my fiancee, YuanXue Liu. I want to thank her patient with me and the support through these years of my studying. Her love enabled me to face up to difficulties and make me the person I am today. Also my supervisor Willie Smit, I never could have done this without his patient guide and help. I'd also like to thank my parents, for all the financial support and encouragement throughout these years of study abroad. All great wishes to you.

Contents

List of Figures

List of Tables

Nomenclature

Variables

w	hour angle	[rad]
t	hours	[h]
α_s	solar altitude angle	[rad]
α_{bias}	elevation bias angle	[mrad]
γ_s	solar azimuth angle	[rad]
γ_{bias}	azimuth bias angle	[mrad]
δ	solar declination angle	[rad]
Δ_e	offset on e axis	[m]
Δ_n	offset on n axis	[m]
Δ_n	offset on n axis	[m]
ε_{pte}	Pedestal tilt errors on e-axis	[mrad]
ε_{ptn}	Pedestal tilt errors on n-axis	[mrad]
ε_{no}	mirror alignment non-orthogonality errors	[mrad]
θ_i	incidence angle	[rad]
μ	mean	[ ]
σ_i^2	Variance of input	[ ]

Vectors and Tensors

C_Y	Variance Matrix of output
C_X	Variance Matrix of input
F_X	Jacobian matrix of input
P_{end}	Point at end of the line
P_{start}	Point at start of the line
R	Rodrigues Rotation Formula
R_e	counter-clockwise rotation matrix around axis e
R_n	counter-clockwise rotation matrix around axis n
R_z	counter-clockwise rotation matrix around axis z
$\hat{e}$	Euler vector

$\hat{h}$	heliostat normal unit vector
$\hat{s}$	Solar unit vector
$\hat{r}$	reflect unit vector

Subscripts

E	East
H	Hypothesis
N	North
S	South
W	West
h	heliostat
i	ideal
s	solar

Abbreviations

CSP	Concentrating solar power
DNI	Direct normal irradiation
PV	Photovoltaic systems

Chapter 1

Introduction

1.1 Background

1.1.1 Renewable Energy

Energy is the basis of social development and economic growth. Societies are becoming more and more dependent on energy. However, conventional energy sources, such as fossil fuels, will at some point be in short supply. These energy sources are also often a source of pollution. For these reasons, the world looks to renewable energy as the energy source of the future.

As Figure 1.1 shows, the main renewable energy sources are wind, biomass, ocean tides and currents, hydropower and solar energy. The Renewables 2015 Global Energy Status Report states that only 23% of the global electricity production comes from renewable sources. There is still much room to expand the production of electricity from renewable sources.

Nuclear power can play a significant role in the energy market. However, the use of nuclear power is often controversial. Hydropower accounts for 17% of all renewable electricity sources. It is much cleaner and more efficient than fossil fuel power plants. The downside to hydropower is that it may require a dam to be built which will change the natural environment. Wind power and solar photovoltaic systems (PV) are clean and the environmental impact is minor compared to fossil fuel power plants. What is more, wind power plants can be built both onshore and offshore. However, electricity from wind power and PV cannot be generated on demand. The main limitation of using biomass as an energy source, is that it has a low conversion rate and requires large amounts of biomass to generate significant amounts of power.

Concentrating solar power (CSP) plants are becoming a viable option to produce electricity in a renewable way. It has the added benefit of being dispatchable, in other words, the plant can produce electricity on demand. This is

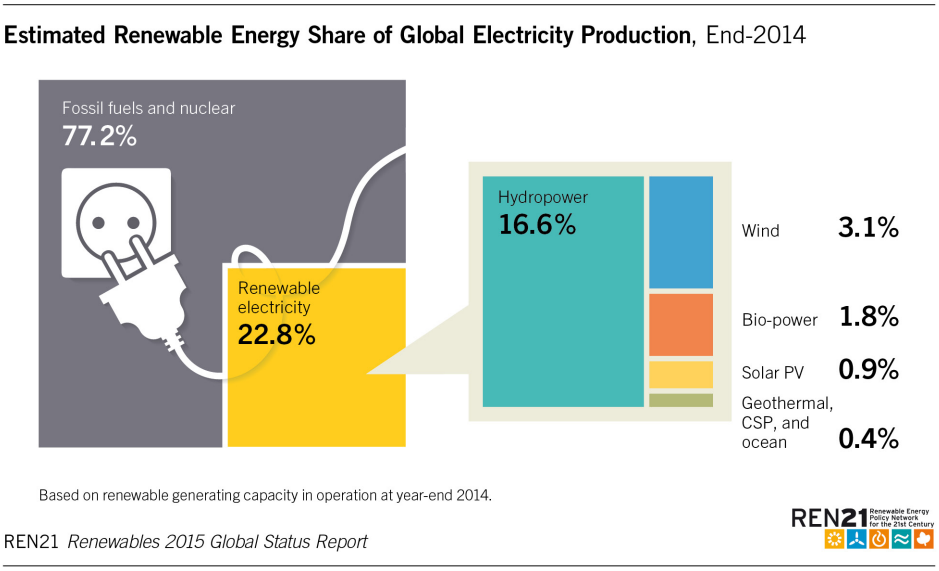

Figure 1.1: The data from Global Electricity Production (Ren21, 2015) shows that renewable energy sources make up around 23% of the total energy production. Hydropower is by far the largest renewable energy source.

possible by storing thermal energy in molten salt tanks.

This chapter starts by giving an overview of renewable energy and discussing concentrating solar power systems in general. After that, it will discuss what a heliostat is, why it is important and how it is calibrated. Lastly, this chapter will discuss the application of the error propagation model to heliostats.

1.1.2 Solar Energy

In some sense, the sun is providing our planet with nearly unlimited solar energy. When sunlight is entering the earth, some of it is absorbed and scattered by the atmosphere, while the remaining sunlight hits the earth's surface.

Solar energy systems mainly use direct normal irradiation (DNI) to generate electricity and not diffused radiation.

Energy from the sun can be used directly by means of PV or CSP, or in-

directly by means of wind power or hydropower.

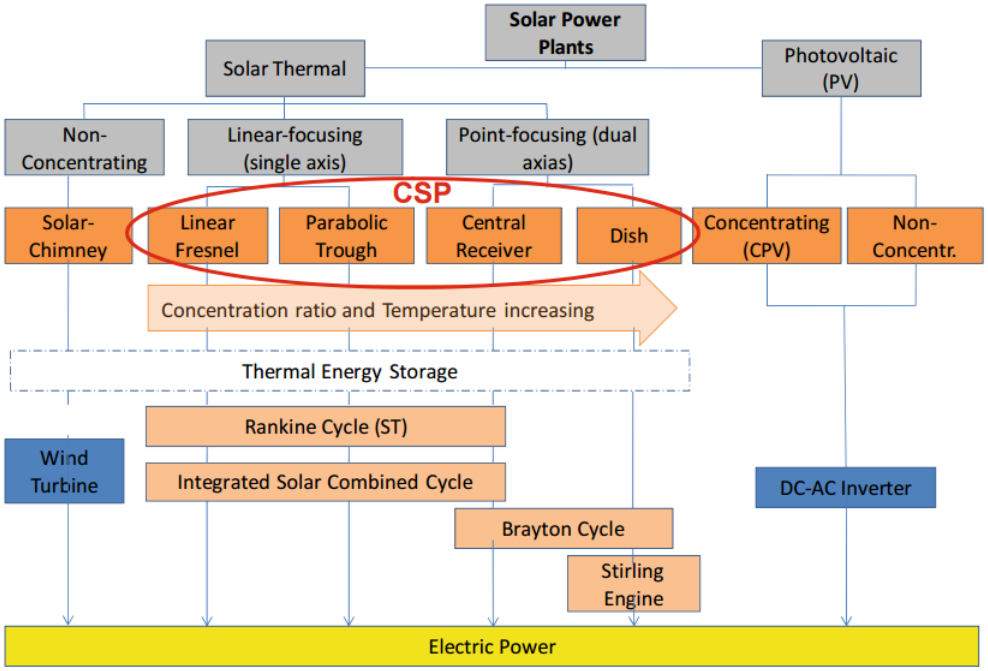

Figure 1.2: Solar power plants can be classified in different ways (Malan, 2014). Concentrating solar power (CSP) includes four types of solar power plants. Concentrating solar power technologies use some method to concentrate solar radiation in order to heat a working fluid.

There are different types of solar power plants. Small-scale solar power plants mainly use PV to generate electricity, while large-scale power plants normally use solar thermal energy to generate electricity. Figure 1.2 shows a useful classification of solar power plants.

1.1.3 Concentrating Solar Power

This section gives a brief view of CSP systems before moving to details of heliostats.

In general, CSP plants concentrate solar rays to heat a working fluid to high temperatures. Heat from the working fluid can be used to generate electricity or it can be stored in molten salt tanks. Unlike other renewable technologies, CSP can produce electricity continuously and steadily by using stored heat. CSP systems consist four main parts:

- The collection (reflector), which concentrate sunlight to a receiver. This can be lenses or mirrors, and are discussed later in details.
- The receiver, which converts the concentrated sunlight to heat and transfer this heat to a working fluid.
- Heat exchanges and storage units, where steam is generated from the working fluid or the heat is stored in molten salt tanks.
- The power cycle, which in many cases is the same as those of conventional thermal power plants.

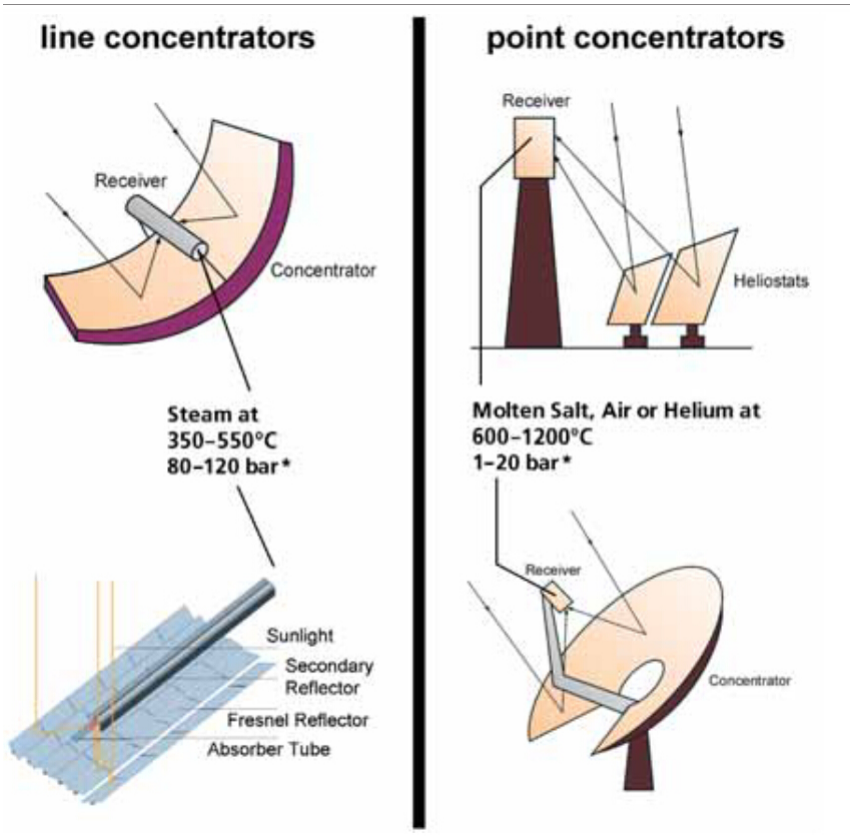

Figure 1.3: The four domain technologies used in CSP are shown here (Müller-Steinhagen and Trieb, 2004). Top left shows a parabolic trough; bottom left shows a linear Fresnel; top right shows a solar tower with a central receiver and bottom right shows a parabolic dish.

As Figure 1.2 shows, there are four dominant CSP technologies (see also Figure 1.3).

- Parabolic Trough.

- Linear Fresnel.
- Parabolic Dish.
- Solar Tower/Central Receiver.

The parabolic trough and linear Fresnel are line concentration systems, using a trough-like mirror as the reflector that concentrates sunlight on a tube receiver. The working fluid is heated as it flows through the tube receiver. These systems are usually designed to track the sun along one axis, which is usually the North-South direction. Compared to other CSP technologies, the parabolic trough and linear Fresnel technologies cannot reach very high working fluid temperatures.

The parabolic dish is a point concentration system. It uses a satellite-like mirror dish as the reflector to concentrate sunlight to a point where the receiver is positioned at. This system is designed to track the sun in two-axis. It has the highest concentration ratio and conversion efficiency of all four CSP technologies. Dish engine systems are normally smaller in scale than line concentration system. Because of their size, they are particularly well suited for decentralized power supply and remote, stand-alone power systems (Müller-Steinhagen and Trieb, 2004).

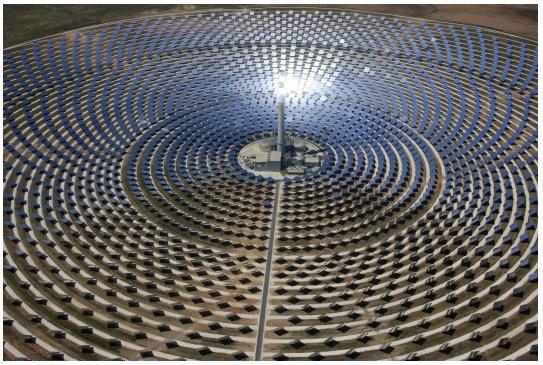

Figure 1.4: An aerial photo of the 19.9 MW Gemasolar Central Receiver CSP plant.

Figure 1.4 shows a central receiver plant and Figure 1.5 illustrates how it works. The central receiver is in a sense similar to the parabolic dish system. Instead of the receiver being surrounded by a dish, it is surrounded by hundreds or thousands of reflectors or heliostats that concentrate sunlight on the receiver that is mounted at the top the tower.

Each heliostat is controlled to reflect solar radiation from the sun. A heliostat

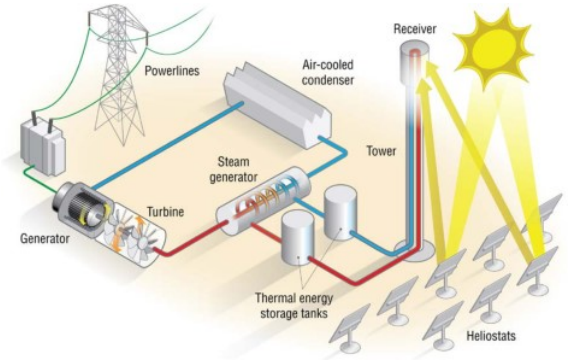

Figure 1.5: Basic subsystems of a molten salt power tower (Kearney, 2014)

can rotate in two dimensions to ensure the reflected rays hit the receiver. The receiver absorbs the sunlight and transfers it to the working fluid. The heat is then stored or used for generating electricity. Central receiver technology is competitive CSP system, as it can achieve high temperatures with little heat loss.

There are many opportunities for CSP in the global market, such as in China, India, Australia, South Africa and so on. China, as a developing country, has a huge energy demand. It is now suffering from air pollution that makes it difficult to build more fossil fuel based power plans. The Chinese government has a series of policies to support renewable energy. However, because this field develops so quickly, the policies are out dated. Government support is required for developing CSP plants in China.

1.1.4 Heliostat

The heliostat is the reflector of a central receiver system. It has to track the sun so that the reflected rays hit the central receiver. It is a key component in a central receiver system. Various companies are developing different heliostat structures. There are no standard sizes of heliostats, their size vary from $1m^2$ to $130m^2$. Figure 1.6 shows one of the 10600 heliostats in the Atacama-1 CSP plant.

Heliostat fields occupy a large area and are expensive. Figure 1.7 illustrates the breakdown of the total installation cost of a central receiver system, in which solar field costs more than 25%.

A heliostat consists of a mirror or a set of mirrors, a sun tracking mechanism and motors or mechanical mechanisms to move the mirror. Those devices are controlled by a computer system that constantly moves the heliostat to keep

Figure 1.6: An Heliostats of PS10 (Abengoa).

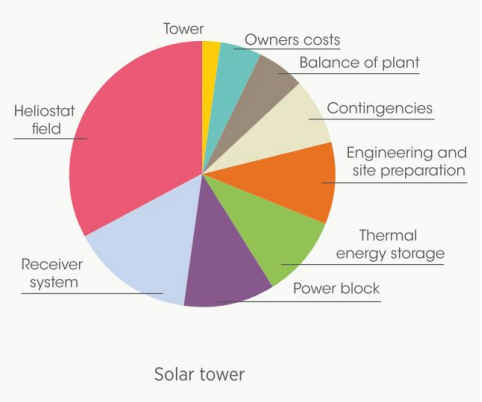

Figure 1.7: Total installed cost breakdown solar tower CSP Plants in South Africa (Hoffschmidt *et al.*, 2012).

the reflected sunlight on one spot on the central receiver.

In a central receiver system, there are two ways to control heliostats, close-loop control and open-loop control. Close-loop control can use a camera mounted near the receiver to look back at the heliostat field. It gives feedback to the heliostats. However, the accuracy of such a system does not provide satisfactory results. The main reason for this is that the camera cannot be placed in the receiver, because it is too hot. Instead, the camera is placed on the edge of the receiver, where it can only measure spillage from the heliostats, not the actual position of the reflected rays.

Another way to achieve close-loop control is to install a sensor on each heliostat to collect parameters in real time. However, it is too expensive to install thousands of sensors. To achieve the required accuracy with open-loop control, it is necessary to have a very accuracy model of each heliostat. Given the date and time of day, it is possible to determine the position of the sun accurately using mathematical formulas. The open-loop control system then sets the orientation of the heliostat based on the sun's position and the heliostat model. The actual point where the reflected rays hit the central receiver is not measured. Almost all commercial CSP plants use open-loop control of the heliostats.

1.1.5 Calibration

As most central receiver system use open-loop control of heliostats, calibration of the heliostat becomes critical. There are different ways to calibrate the heliostats. One method use heliostat pointed to the sun following the information from the sun sensor or a sun position algorithm result. Because of the errors exist, heliostat cannot point to the exact position where the sun should be. The difference can be used to estimate the errors in the heliostat. Then those errors correct heliostat tracking model to get a better result in an open-loop control system. A popular way is to track the reflected rays on a target plane and use the difference between the reflected point and the center of the target plane to estimate errors in the heliostat model.

1.2 Motivation

The previous sections have shown that the cost of heliostats make up a big portion of the total plant cost. It was also argued that it is important to have a properly calibration heliostat model to achieve the required open-loop control accuracy. For these reasons, a lot of research effort is put into heliostats, firstly to reduce their cost but also to improve their accuracy.

1.3 Problem Outline

After calibration a heliostat should be able to reflect solar rays onto the center of the target. However, with calibration errors, the solar rays will not be reflected to the exact point on the target. This work is an investigation into the effect of calibration errors on the control accuracy of a heliostat

1.4 Objectives

This thesis aims to give a better understanding of the heliostat error model, the calibration results and their influence on open-loop control accuracy. It aims to do so by applying error propagation law to the heliostat model.

The usefulness of error propagation will be demonstrated by answering several issues related to heliostats, such as:

- Central receiver plants are usually built in some dry area. However, after heavy rain in such an area, the ground may move ever so slightly, which will cause the heliostat to tilt in some direction. It is needed to quantify the effect of such tilting on the control accuracy.

- How could the position of the reflected rays on the target be found?
- What is the sensitivity of each error in the model? Which error has the biggest affect on the reflected rays?
- How does the solar vector effect reflected rays with different errors?
- How does the position of the heliostat relative to the tower affect the control accuracy?

1.5 Methodology

Due to the objectives, the research methodology can be summarized as following:

- Do a literature survey of previous work on heliostat calibration.
- Derive and validate an error model of a heliostat.
- Apply the error-propagation law to the heliostat error model and validate the answer.
- Apply the model to answer several questions related to the heliostat error model.

1.6 Scope

This thesis uses a heliostat error model and applies the error propagation law to this model. It uses an an eight parameter error model of a heliostat similar to the work of (Malan, 2014). It applies the error propagation method on the error model to get an error propagation model. It uses the error propagation model to answer some questions about the relationship between errors in the heliostat model and the control accuracy.

1.7 Outline

Chapter 2 contains a literature review of research on the central receiver system, especially heliostats. It also looks at solar position, solar tracking, heliostat calibration and heliostat error. The chapter ends with a literature review of error propagation and hypothesis testing.

Chapter 3 validates the heliostat error model by comparing it with the work of Malan (2014). This error model is used in Chapter 4 to derive an error

propagation model.

Chapter 4 derives the equations of the error propagation model, which illustrates the error uncertainties and distribution of the reflected rays on the target plane. The error propagation model is validated by using hypothesis testing with data generated from a Monte Carlo method. The error propagation model can be used to answer questions in Chapter 5.

Chapter 5 applies the error propagation model to answers questions related to the heliostat error model.

Chapter 6 concludes the thesis.

Chapter 2

Literature Review

This chapter first discuss the central receiver system. After that, it explains the fundamentals of the solar position. The discussion then moves to heliostat calibration and the heliostat error model. It ends with a discussion of error propagation.

2.1 Central Receiver System

2.1.1 Development

Central receiver systems were firstly developed in the early 80's, since then, more than 10 central receiver power plants have been built. The 377 MW Ivanpah solar power facility also called Solar One, located in California's Mojave Desert, is the world's largest solar thermal power plant project to 2012 (Gallego *et al.*, 2012). This power plant was built with steam power tower technology to demonstrate its feasibility. Though the output of Solar One was lower than expected, it provided a significant amount of data to help researchers redesign Solar Two.

2.1.2 Heliostat Field

The design and study of first-generation heliostats have begun at the end of the 1970s. Heliostat fields strongly affect the performance of central receiver systems (CRS). Not only should the heliostat be structurally well-designed but the field layout should also be carefully planned to reduce blocking and shading(Behar *et al.*, 2013).

The structural design of heliostats need to consider wind loading, the size of the heliostat and cost. Kolb *et al.* (2007) found from a cost analysis that heliostats should be bigger than $150m^2$. However, for that size, wind load has a significant influence on the heliostat that makes it vibrate heavily and

increases maintenance cost (Wu *et al.*, 2010). For that reason, some heliostats were designed with a gap (0-40mm) on their surface (Wu *et al.*, 2010).

As chapter 1 said, A heliostat field cost around 25% of installation cost, what's more, it takes around 50% of the total investment which including installation cost, material cost and research cost etc. Besides it accounts for 40% of the energy losses (Behar *et al.*, 2013). For this reason, some different field layouts methods have been developed.

2.1.3 Receiver

Figure 2.1 shows four different types of central receiver towers. The tower has two main parts. The first one is the receiver that set on the top on the tower. It absorbs reflected sunlight and converts it to heat. In a central receiver system, the receiver can achieve temperatures up to 1000°C. The second part is calibration target, which is mounted below the receiver. It has various forms, but is normally a white board.

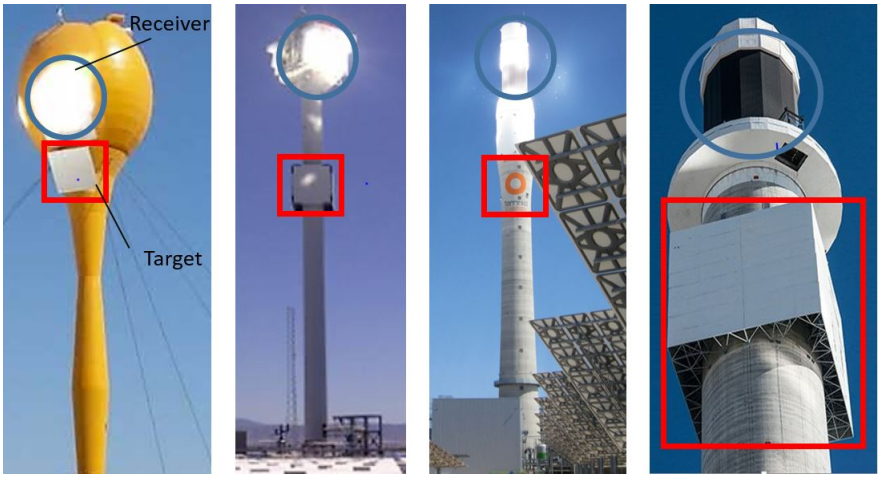

Figure 2.1: The tower of a central receiver system consists of two parts: a receiver and a calibration target. From left to right: AORA's Solar Flower Tower, Sierra SunTower, Torresol Gemasolar power tower, Solar Two tower.

The receiver can be classified into one of three groups: volumetric receivers, cavity receivers and particle receivers. Behar *et al.* (2013) discuss research relevant to receivers.

2.1.4 Control System

The open-loop heliostat control system determine the sun's position from mathematical formula and then calculate the required orientation of the heliostat. For an open-loop control system, performs adequately provided the heliostat is calibrated.

Baheti and Scott (1980) designed a self-calibrating controllers for heliostats. It is the normal way to of controlling heliostats. The controller uses a linear equation to establish error model. The controller has been designed operating in two ways. In calibration model, it is using least-squares algorithm to estimate parameters for the system. In tracking model, it uses parameters come from calibration model to reflect sunlight to the target. Aiuchi *et al.* (2006) used a photo-sensor fitted to the mirror of the heliostat that tracks the sun. With this step they have achieved heliostat control with an error of 0.6 mrad in clear weather. However, the sensor has bad performance during cloudy weather and they got larger errors during this time. Kribus *et al.* (2004) considered a closed loop control system. Four CCD cameras were plated around the target, that detects heliostats errors in real-time and automatically correct these errors. Their algorithm can reach an accuracy of $0.1 - 0.3$ mrad. However sophisticated algorithm may be needed to avoid overshoot and oscillations when increase system speed. On the other hand, image analysis software requirements to extension to a large field with many heliostats also becomes the limits of this control method. Ulmer *et al.* (2011) designed an automatic measurements system to detect heliostat errors. Malan (2014) designed software and hardware for a heliostat field control system. He derived an error model and compared it with Stone *et al.* (1995). With his control system, heliostats can get a reflected image error at 1.94 mrad.

2.2 The Solar Position

Open-loop heliostat control requires an accurate position of the sun. This section gives an overview of how the sun moves through the sky, how the sun can be tracked and also how the position of the sun can be calculated.

2.2.1 Earth-Sun Geometry

M. (2006); Pidwirny explains the fundamentals about the relationship between the earth and sun. Stine and Geyer (2001) give more detail about how to determine the solar vector from the earth-sun geometry.

2.2.1.1 The Earth Viewed from the Sun

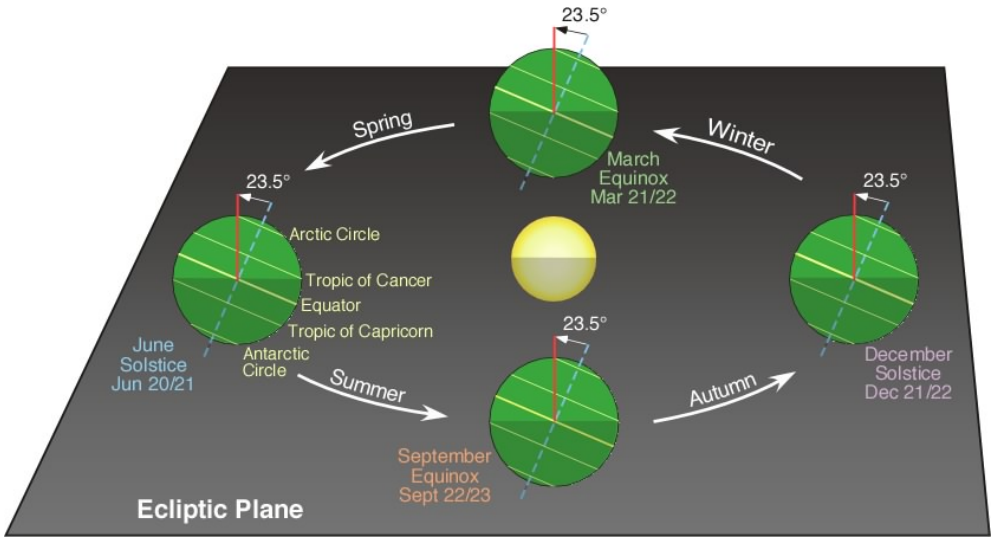

Figure 2.2: A view of the earth in its orbit about the sun (M. (2006); Pidwirny)

The earth rotates around its axis and each rotation lasts around 24 hours. When observing from the north side of the earth in universe, the earth rotates from the west towards east surround sun.

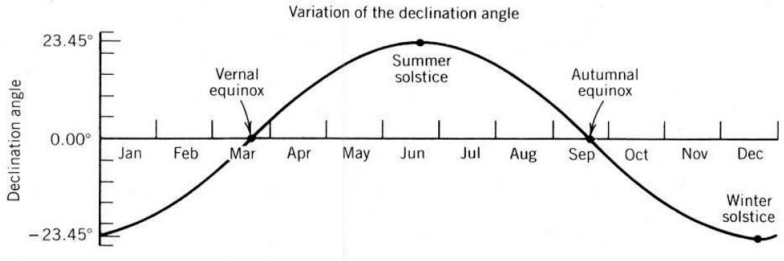

Figure 2.3: Angle of the sun's declination throughout the year. (Swinton, 1920)

The earth travels around the sun in an orbit which is not circular but elliptical. The earth takes 365.26 days to complete one cycle around the sun. Figure 2.2 illustrates the positions in the earth's orbit. On January 3, perihelion, the earth is closest to the sun (147.3 million km) and on July 4, or aphelion, the earth is furthest from the sun (152.1 million km). The average distance between the earth and the sun over a one-year period is around 149.6 million km. The ecliptic plane is defined as the plane which contains the earth's orbit around the sun. In addition, the plane that includes the earth's equator is called the equatorial plane. The angle between ecliptic plane and equatorial

plane is called the declination angle (δ). Figure 2.3 illustrates how the declination angle changes during the year. On the June solstice this angle is equal to 23.45° and on the December solstice it is equal to -23.45°.

2.2.1.2 The Sun Viewed from the Earth

For an observer on the earth, the sun's orbit is a segment of an ellipse. From the sunrise to sunset, it moves at a constant speed around 15 degrees per hour. As shown in Figure 2.2, Q is the observer on the earth, the center of the orbit is on the axis that go through the observer and the north star. The rotational velocity of the earth is not constant, but varies slightly over time. Moreover, for the different seasons and locations of an observer, the height of the orbit is different. Swinton (1920) gives an algorithm to accurately calculate the position of the sun based on time and position of the observer.

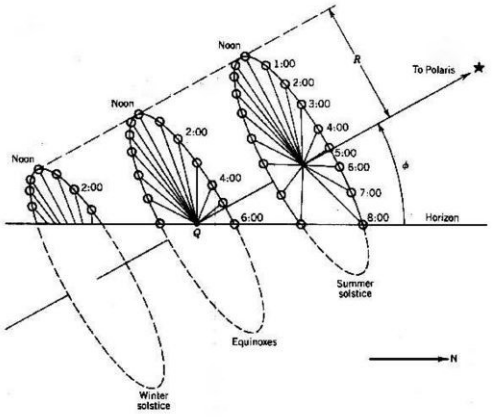

Figure 2.4: A geometric view of the sun's path as seen by an observer at Q. Each disc has radius R. (Swinton, 1920)

2.2.2 Solar Tracking Technology

An observer on the earth can use equipment to accurately determine the sun's position in real-time. There are different types of classification in research. In generally, solar trackers are classified in two ways, active and passive. Active solar trackers work on the principle that use motor change the angle of trackers to follow the sun actively. Whereas passive solar trackers using a balance of forces to track the sun passively.

Poulek and Libra (1998) developed a new tracking stand to combine both

higher efficiency of active trackers and simple design of active trackers. Clifford and Eastwood (2004) discussed a range of solar trackers in both positive and active and showed a new designed novel passive solar tracker. Rubio *et al.* (2007) indicate that "regarding control units, the main types of solar trackers are: passive, microprocessor and electro-optical controlled units." For the first type it does not use any electronic control or motor. For the second one, it uses a mathematical formula to predict the sun's movement and need not sense the sunlight. Rubio *et al.* (2007) also indicate a search method to let tracker find the sun position when tracker loses the sun position that makes sensor has no feedback. Finally, the electro-optical controlled units that use the information of some sensor to estimate the sun's real position then use that information in the control algorithm. Mousazadeh *et al.* (2009) indicate the classification of the solar tracker and shows more detail in the active solar tracker. Rizk and Chaiko (2008) shows "the potential system benefits of simple tracking solar system using a stepper motor and light sensor." Lee *et al.* (2009) indicate another classification of solar tracker that classifies them in open-loop and close-loop. Malan (2014) shows classification and example in the Table 2.1.

Table 2.1: Classification and examples of solar tracking mechanisms (Malan, 2014)

Passively powered mechanisms		Actively powered mechanisms
Open-loop tracking	Clockwork mechanisms	Microprocessor-based solar algorithms
Closed-loop tracking	Trackers using thermal expansion actuators	Electro-optical feedback sensors

2.2.2.1 Passive solar tracker

Passive solar trackers normally have a simple design, using a balance of forces to track the sun. If it does not point directly at the sun, an unbalanced force would correct it. Normally passive solar tracker have a slower response and is cheaper compared to active solar trackers. Some of the passive solar trackers make use of the thermal expansion of a matter (usually Freon) or on shape memory alloys (Mousazadeh *et al.*, 2009). Clifford et al. presented a novel passive solar tracker modeled with a computer system.

2.2.2.2 Active solar tracker

Mousazadeh *et al.* (2009) categorized active solar trackers into four categories:

- Microprocessor and Electro-optical sensor based.
- PC controlled date and time based.
- Auxiliary bifacial solar cell based
- A combination of three above.

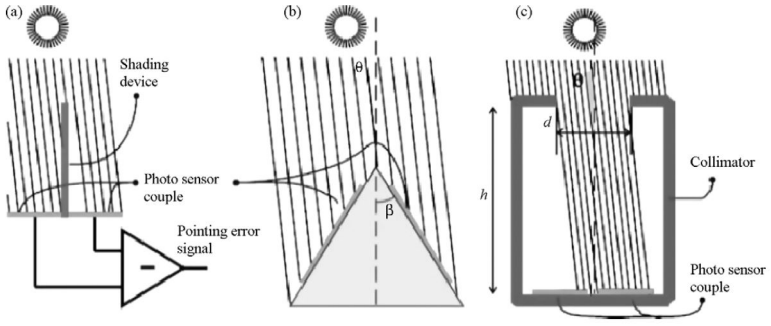

Figure 2.5: Shade balancing principle (a) sun-pointing sensors (b) tilted mount of photo sensors (c) precise sun pointing by means of a collimator (Mousazadeh *et al.*, 2009)

Microprocessor and electro-optical sensor based systems measure the difference between two electro-optical sensors to determine if the sensor is pointing directly at the sun. Figure 2.5 shows three possible set-ups. Sensor (a) in figure 2.5 shows a light shade sensor, which can be used to drive a motor that orientates the sensors to point directly at the sun. Sensor (b) detects light on two sides of a triangle. Rizk and Chaiko (2008) discussed details about this sensor. Sensor (c) uses slit and two photo sensors to find the direction of the sun relative to the sensors.

PC controlled, date and time based tracker is widely used and researched. It uses an algorithm to calculate the position of the sun by given the day number in computer and tracker's position from GPS. Then based on the consequences from algorithm, computer can control all heliostats point to the right direction. There are many research papers refer to the solar position. It will discuss what they are and how they work in the next section.

The auxiliary bifacial solar cell based tracker is described by Poulek and Libra (1998). It uses a PV cell to collect solar energy which drive DC motor to rotate the whole system. The system is shown in figure 2.6. When the solar rays are perpendicular to the collector, the PV panel does not absorb any sunlight. This means that no power is supported to the motor and the rotation of the collector stops.

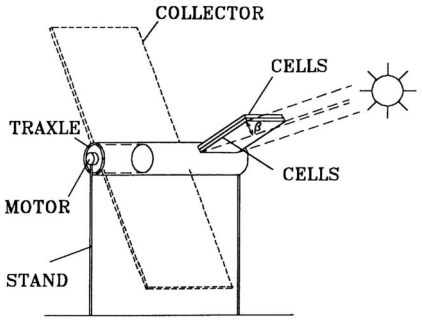

Figure 2.6: Horizontal axis tracker.(Mousazadeh *et al.*, 2009). The cells collect sunlight to generate electric power which supports motor. Then motor changes the angle of whole system until cells perpendicular to the sunlight, in which position, the collector can receive maximum solar rays.

2.2.3 Solar Position Algorithm Accuracy

The position of the sun in the sky can also be calculated instead of measured. The calculated position is for almost all practical applications accurate enough. Many research papers refer to the calculation of solar position. Sun position algorithms have been widely used in CSP plants. In general, the controller calculates the sun's position with a mathematical algorithm and control the orientation of the reflector accordingly. However, central receiver system that have a large number of heliostats, each heliostat controller should be cheap. The implementation of the controller should find a balance between accuracy, complexity and cost.

Some algorithm only uses the day of the year and the declination angle to calculate the sun's position (Cooper, 1969; Spencer, 1971; Swift, 1976; and Lamm, 1981;) others use more complex algorithms (William B. Stine and Michael Geyer (Swinton, 1920)) that use latitude, day number and solar time to calculate the sun's position. There are also some other algorithms exists: Walraven, 1978; Priman and VantHull, 1978; Michalsky, 1988; Blanco(PSA), 2001; Lbrahim Reda,2004; Roberto Grena, 2007; Reda and Andreas(SPA), 2008;

Table 2.2 shows the accuracy of some solar position algorithms. The solar Position Algorithm (SPA) by Reda and Andreas, 2008 has the best accuracy with a maximum tracking uncertainty of 0.0003 degrees.

Table 2.2: Some author with their algorithm's year,uncertainty

Author(s)	Year	Algorithm Uncertainty (degree)
Spencer	1971	0.25
Pitman and Vant-Hull	1979	0.02
Walraven	1979	0.013
Michalsky	1988	0.011
Blanco-Muriel et al.	2001	0.008
Grena	2007	0.0027
Reda and Andreas	2008	0.0003

2.2.4 Solar Vector

The solar vector is generally used to describe the position of the sun. It is calculated for each individual heliostat in a central receiver plant, so that the heliostat reflects the sun onto the central receiver. The algorithm presented here calculates the unit solar vector ($\hat{s}$) instead of the solar azimuth (γ_s) and the altitude angle (α_s). The derivation that follows is adapted from William B. Stine and Michael Geyer (Swinton, 1920). As solar design purposes, however, here only has an approximation accurate within about 1 degree.

1. Express time t in hours where $t \in [0, 24)$. The hour angle (w) can be described by:

$$w = 15(t - 12) \tag{2.1}$$

2. Set N as number of days since January 1 (if the year is a leap year, add one day for the date between 1 March to 31 December). The declination angle (δ) can be calculate as:

$$\delta = \arcsin(0.39795 \cos[0.98563(N - 173)]) \qquad (rad) \tag{2.2}$$

3. Set the latitude angle (ϕ) of the observer's position. The sun altitude angle (α_s) can be expressed as:

$$\alpha_s = \arcsin(\sin(\delta)\sin(\phi) + \cos(\delta)\cos(w)\cos(\phi)) \tag{2.3}$$

4. The solar azimuth angle (γ_s) can be found by:

$$\gamma_s^{''} = \arccos(\frac{\sin(\delta)\cos(\phi) - \cos(\delta)\cos(w)\sin(\phi)}{\cos(\alpha_s)}) \qquad (rad) \tag{2.4}$$

If $\sin(w) > 0$

$$\gamma_s = 2\pi - \gamma_s^{''} \tag{2.5}$$

Else $\sin(w) \leq 0$

$$\gamma_s = \gamma_s'' \tag{2.6}$$

5. The solar vector $(\hat{s})$ can now be expressed as:

$$\hat{s} = s_z\hat{z} + s_e\hat{e} + s_n\hat{n} \tag{2.7}$$

where $s_z = \sin(\alpha_s)$, $s_e = \cos(\alpha_s)\sin(\gamma_s)$, $s_n = \cos(\alpha_s)\cos(\gamma_s)$

2.3 Heliostat Calibration

Each heliostat in a CSP plant has it's bias to reflect the solar rays to the receiver. Those bias need to be calibrated to ensure each heliostat reflects solar rays to the receiver accurately. Otherwise, the efficiency of solar power plant will drop heavily. In general, heliostat calibration is gathering the information about how heliostat works and where the bias are. Then the control system can adjust the angle of each heliostat to compensate the bias.

Several calibration methods have been implemented in central receiver heliostat control system. For gathering information about bias on heliostats, some method install sensors on each heliostat to measure the bias, alternatively, some method use a camera to capture the reflection image on calibration target plan, then using different algorithm to calculate the parameters of heliostats. The calibration method in most papers are based on Berenguel *et al.* (2004).

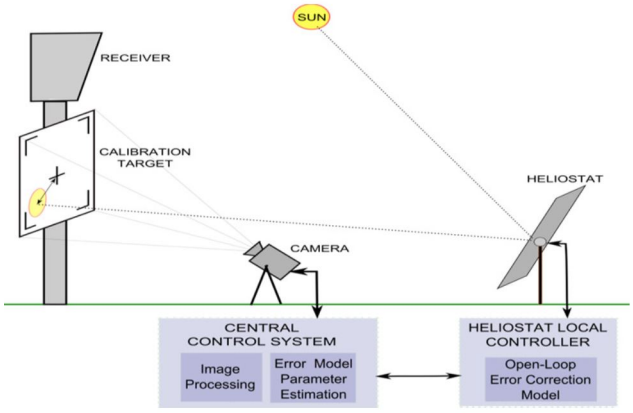

Figure 2.7: Concept of operation of the heliostat field control system(Malan, 2014)

Most heliostats calibration methods ask for the sun's position to calibrate he-

liostats. Based on different methods to calculate the sun's position. There are different method to calibrate helisotats.

- For passive solar tracking system, it actually can not actively control variables about the system. Besides, it is hardly used in Central Receiver System.
- Sensor based and PC controlled date and time-based, calibration method can be either close-loop or open-loop, due to the cost, most central receiver system does not choose this option.
- Sensorless, PC controlled date and time based, which calibration method almost depends on the mathematical model. In some case, this system asks for GPS to get date and time information.

There is little information publicly available on commercial heliostat calibration techniques. Most papers refer to the calibration method described by Berenguel *et al.* (2004) which is a sensorless method. Malan (2014) illustrates this method using Figure 2.7. It is a close-loop calibration process. Figure 2.8 shows the reflect image caught by camera on calibration target plane. First it uses the camera to capture reflected image on the calibration target. After that it compares the center of the target with sunbeam centroid, and calculated the sun's position by an algorithm. After that it uses an algorithm to calculate errors on the heliostat. Then offset correction on the model. After finish all above, it does the iteration to figure out best offset correction. Malan (2014) also design and model a control system for a 5 MW_e pilot based on this method. Alternatively, eSolar's calibration method is different from other. To calibrate a large number of heliostats, eSolar build several target tower around the heliostat field that can let a number of heliostats do the calibration at the same time.

2.4 Heliostat Error

Calibration and tracking of heliostats in central receiver system has become a key factor for cost reduction of CSP plants. Baheti and Scott (1980) illustrate that the angular accuracy for large heliostat fields must be approximately 0.1 degrees.

The error sources of heliostat tracking are dealt with by Stone *et al.* (1995). The authors discusses about the geometrical errors that reduce heliostat tracking accuracy in Solar Two. After that, authors identified three dominant error sources:

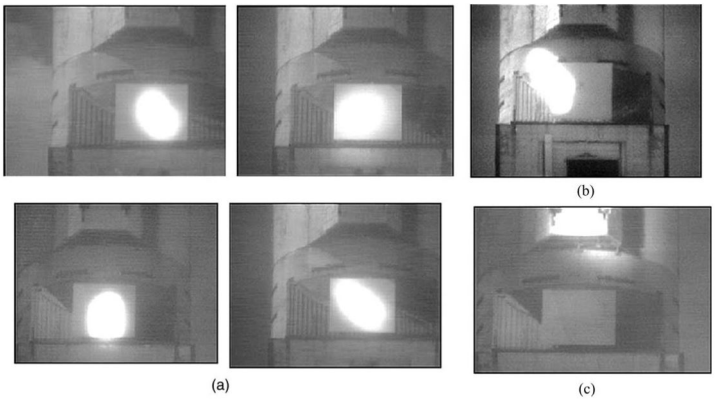

Figure 2.8: Details of the calibration target and the different shapes of the reflected image of the sun projected by the heliostats. (a) centered ellipsoids the orientation of the shape changes during the day. (b,c) Ellipsoids are out of the target due to aiming errors (Berenguel *et al.*, 2004)

- Azimuth axis tilt errors which was main error sources from heliostat was installed. Those errors are come from the heliostats' axis tilted.
- Mirror alignment canting errors. It occurs when the heliostat mirrors' normal vector are not pointing the same direction with the normal vector to the heliostat's local elevation plane defined by the gear drive assembly.
- Encoder reference errors. It comes from the motors on the heliostats which do not work in good condition. Normally it can be easily fixed once noticed.

Freeman (2014) discuss the effect of several errors on calibration and control system in depth. The paper lists 15 errors as shown in Table 2.3.

2.5 Heliostat Error Model

Heliostat error model is a mathematical model that simulate how heliostat reflect solar rays to the receiver. By given errors in specific heliostat the model can shows the reflected solar ray on the target plan. Heliostat error model gives a significant view about how errors affect the reflect solar rays.

There are some error model built by different research. Baheti and Scott (1980) illustrate a mathematical error model including six installation coefficients and drive errors. In his model the difference between commanded and actual drive angles using the coordinate transformation method based on the azimuth-elevation tracking geometrical relationship. Hogan *et al.* (2013) also use the same model in his paper.

Table 2.3: Result of the risk/reward assessment (Freeman, 2014)

Ranking	Error number and description
1st biggest effect	Backdrive of heliostat Low encoder resolution
2nd biggest effect	Gear ratio choice Pedestal tilt Azimuth and Elevation reference angle Non-level terrain
3rd biggest effect	Mirror surface deformations Reflectivity reduction with aging Errors due to wind loading Gear backlash Cable slippage Dimensional tolerances in drive wheel Encoder type
Smallest effect	Reduction of accuracy of sensors with aging Divergence of ref1ected rays from heliostat

Malan (2014) use another model based on Stone *et al.* (1995). A 3D overview with the explanation will be given as following.

2.5.1 Heliostat 3D Overview

A Cartesian coordinate system has been built to illustrate the position of a heliostat and its relationship between target plan in three dimensions. Figure 2.9(left) shows a overview of geometrical heliostat model. An east, north, zenith coordinate system is used in the rest of paper. Sun light reflected by heliostat plan to the target plan on the tower. Figure 2.9(right) shows details of vectors with their azimuth angles(γ) and elevation angles(α) .

- Point B is center of heliostat plan which located at $B(z_B, e_B, n_B)$. Point A is the center of target plan which located at $A(z_A, e_A, n_A)$. In this paper, the bottom of the solar tower is set at the original point that is $O(0, 0, 0)$.
- $\hat{s}$ is solar vector describe the direction of sunlight.
- $\hat{r}$ is the reflect vector that point to the center of target plan.
- $\hat{h}$ is the normal vector of heliostat which perpendicular to heliostat plan.
- Because incidence angle(θ_i) is the angle caused by reflection, this angle between the normal vector and reflect vector is same with the angle between the normal vector and solar vector.

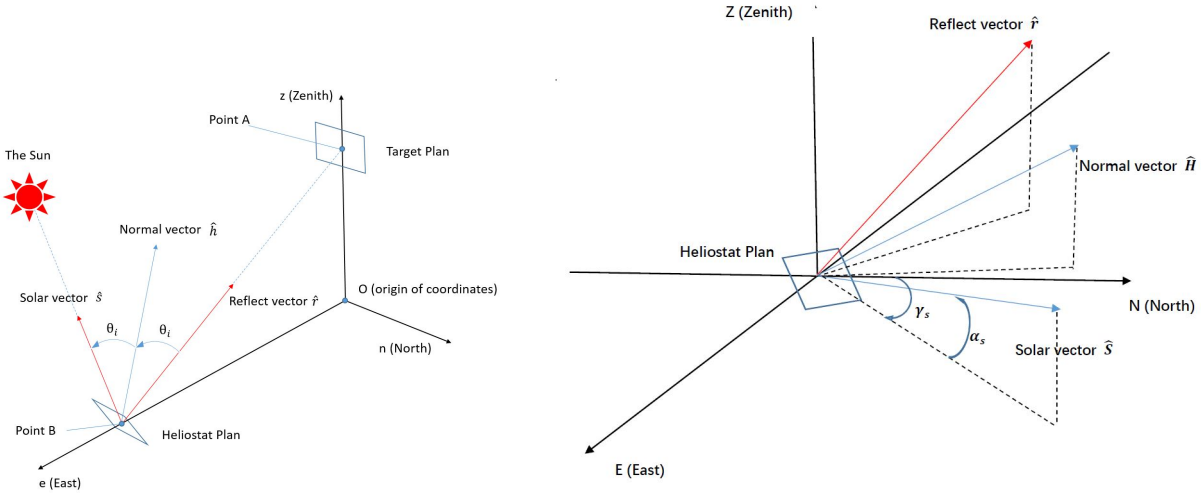

Figure 2.9: Vector and Angle for a heliostat model

In this paper the target plan is face to east, so that the normal vector of target plan(N_{target}) should be $[0, 1, 0]$.

2.5.2 Heliostat Normal vector

Figure 2.9(left) illustrates the relationship between Normal vector of heilostat and incidence angle(θ_i).$\hat{r}$ is the vector from central of the helistat point to the central of target plan. The angle from normal vector to solar vector and from normal vector to reflect vector are same so that:

$$\hat{r} = \frac{(z_t - z_h)\hat{z} + (e_t - e_h)\hat{e} + (n_t - n_h)\hat{n}}{\sqrt{(z_t - z_h)^2 + (e_t - e_h)^2 + (n_t - n_h)^2}} \tag{2.8}$$

$$\cos(2\theta_i) = \hat{s} \cdot \hat{r} \tag{2.9}$$

$$\theta_i = \frac{\arccos(\hat{s} \cdot \hat{r})}{2} \tag{2.10}$$

Because of this model reconstruct each vector after add errors in different angles. Therefore it is necessary to calculate heliostat normal vector by incident angle:

$$\hat{h} = \frac{\hat{r} + \hat{s}}{2\cos(\theta_i)} \tag{2.11}$$

2.5.3 Rotation Matrix

Errors in heliostat affect on heliostat plan which can be seen as rotation around different axes. Following defined different types of rotation matrix.

Rotation Matrix Re perform a counter-clockwise rotation through an angle θ around axis e:

$$R_e = \begin{bmatrix} 1 & 0 & 0 \\ 0 & \cos(\theta) & \sin(\theta) \\ 0 & -\sin(\theta) & \cos(\theta) \end{bmatrix} \tag{2.12}$$

Rotation Matrix Rn perform a counter-clockwise rotation through an angle α around axis n:

$$R_n = \begin{bmatrix} \cos(\alpha) & 0 & -\sin(\alpha) \\ 0 & 1 & 0 \\ \sin(\alpha) & 0 & \cos(\alpha) \end{bmatrix} \tag{2.13}$$

Rotation Matrix Rz perform a counter-clockwise rotation through an angle γ around axis z:

$$R_z = \begin{bmatrix} \cos(\gamma) & \sin(\gamma) & 0 \\ -\sin(\gamma) & \cos(\gamma) & 0 \\ 0 & 0 & 1 \end{bmatrix} \tag{2.14}$$

The plan of heliostat also rotated around it's pedestal, for which Rodrigues Rotation Formula can be used. It describes a rotation around any fixed axis. Fixed axis can be described as Euler vector($\hat{e}$) and θ represent the rotation angle. For helisotat, Euler vector($\hat{e}$) represents heilostat pedestal.

$[\hat{e}]_X$ is 3x3 skew symmetric matrices which shows as following:

$$[\hat{e}]_X = \begin{bmatrix} 0 & e_3 & -e_2 \\ -e_3 & 0 & e_1 \\ e_2 & -e_1 & 0 \end{bmatrix} \tag{2.15}$$

Then rotation(R) of Rodrigues Rotation Formula can be presented as following:

$$R = I_3 \cos(\theta) + (1 - \cos(\theta))[\hat{e}]_X [\hat{e}]_X^T + [\hat{e}]_X \sin(\theta) \tag{2.16}$$

Figure 2.10 shows all rotation matrix in three dimension view.

2.5.4 Errors

There are totally 8 error sources which belong to installation error in this model. They are discussed as following:

1.Bias angle about heliostat plan. It is about the azimuth bias angle(γ_{bias}) and elevation bias angle(α_{bias}) which describe the offset on heliostat. Figure 3.2 shows relationship between those two errors and normal vector of heliostat.

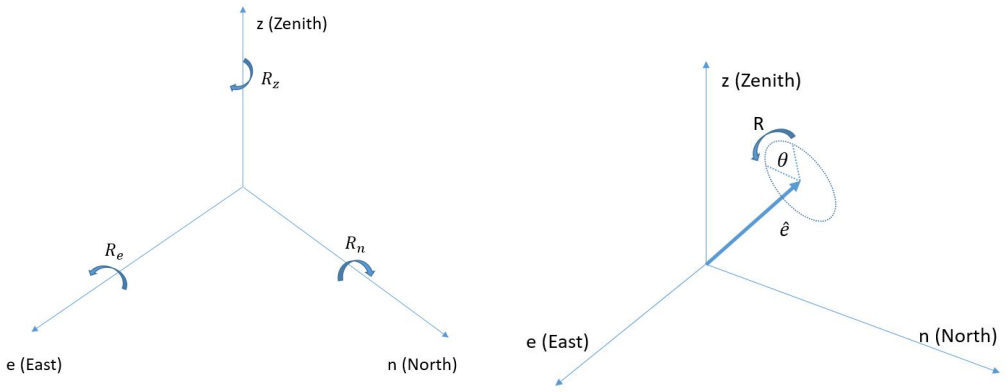

Figure 2.10: Rotation in three dimension view

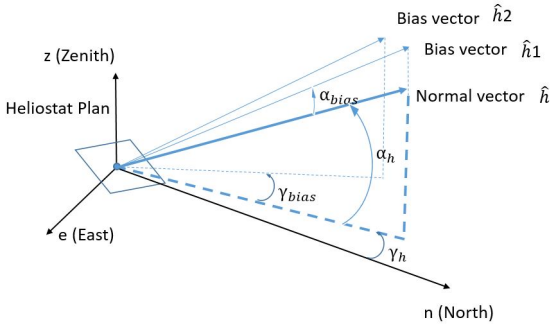

Figure 2.11: azimuth bias angle(γ_{bias}) and elevation bias angle(α_{bias})

2.Pedestal tilt errors indicate the offset in main support of heliostat. Offset can be seen as rotation in two direction, counter-clockwise rotation on e axis(ε_{pte}) and counter-clockwise rotation on n axis(ε_{ptn}). The offset shows in Figure 2.12

3.(ε_{no}) express the mirror alignment non-orthogonality errors. Figure 2.13 shows where the error comes from.

4.Once heliostats have been installed, there will be displacement for each heliostat's position. Due to non-level ground, there are also some offsets on position information. Δ_e, Δ_n, Δ_z represent offset on e axis, n axis and z axis respectively.

2.5.5 Mathematics of Error Model

This section illustrate details of Error Model of a heliostat. All model is based on karel's work(Malan, 2014). Moreover, this model can be set in several steps

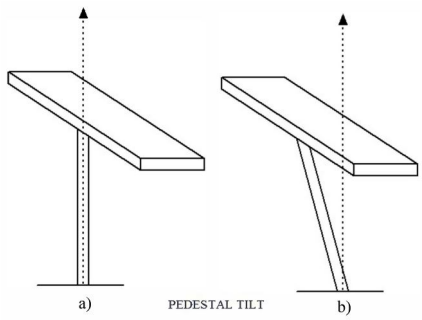

Figure 2.12: (a)shows pedestal without offset. (b)shows pedestal with offset.(Freeman, 2014)

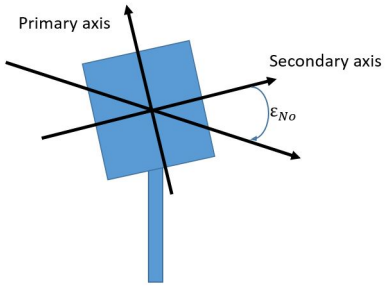

Figure 2.13: Mirror cant error (ε_{no})

as Figure 2.14 shows.

1. Using the solar vector and reflect vector to calculate ideal incident angle.

$$\theta_i = \frac{\arccos(\hat{s} \cdot \hat{r})}{2} \tag{2.17}$$

2. Using ideal incident angle, solar vector and reflect vector, ideal normal vector can be expressed as:

$$\hat{h}_i = \frac{\hat{r} + \hat{s}}{2\cos(\theta_i)} \tag{2.18}$$

3. The azimuth angle and elevation angle of ideal normal vector can be expressed as:

$$\alpha_{\hat{h}_i} = \arcsin(\hat{h}_i(3)) \tag{2.19}$$

$$\gamma_{\hat{h}_i} = \arcsin(\frac{\hat{h}_i(1)}{\cos(\alpha_{\hat{h}_i})}) \tag{2.20}$$

4. Adding bias angle to ideal normal vector:

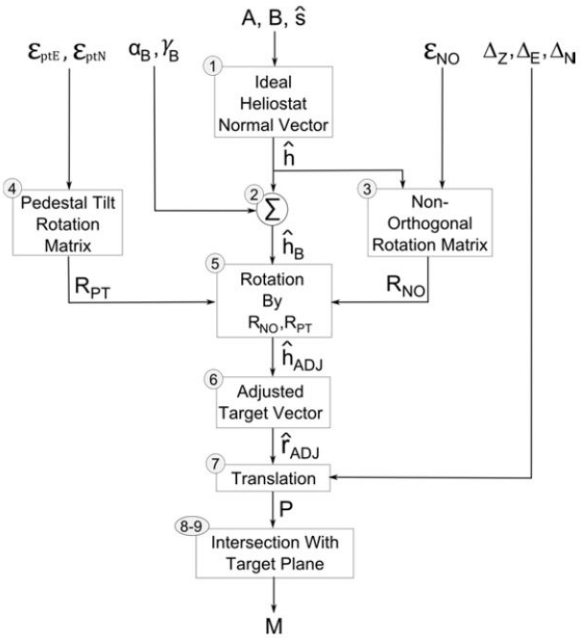

Figure 2.14: Error Model derivation steps(Malan, 2014)

$$\alpha_{\hat{h}_{bias}} = \alpha_{\hat{h}_i} + \alpha_{bias} \tag{2.21}$$

$$\gamma_{\hat{h}_{bias}} = \gamma_{\hat{h}_{bias}} + \gamma_{bias} \tag{2.22}$$

5. The bias normal vector can be found by:

$$\hat{h}_{bias} = \left[\sin(\alpha_{\hat{h}_{bias}}) \quad \cos(\alpha_{\hat{h}_{bias}})\sin(\gamma_{\hat{h}_{bias}}) \quad \cos(\alpha_{\hat{h}_{bias}})\cos(\gamma_{\hat{h}_{bias}})\right] \tag{2.23}$$

6. Bias heliostat normal vector then should be rotated by rotation matrix:

$$\hat{h}_{rotated} = R_e R_n R_z R \hat{h}_{bias} \tag{2.24}$$

7. New incident angle can be expressed as:

$$\theta_{new} = \arccos(\hat{s} \cdot \hat{h}_{rotated}) \tag{2.25}$$

8. New reflect vector can be expressed as:

$$\hat{r}_{new} = 2\cos(\theta_{new})\hat{h}_{rotated} - \hat{s} \tag{2.26}$$

9. If we image the reflected sunlight as a vector. Then the start point of real

reflect vector can be found by adding position offset to the heliostat position:

$$P_{start} = \begin{bmatrix} z_h + \Delta_z & e_h + \Delta_e & n_h + \Delta_n \end{bmatrix} \tag{2.27}$$

10. The end of reflected sunlight vector can be seen as:

$$P_{end} = P_{start} + \hat{r}_{new} \tag{2.28}$$

11. Any point on target plan can be expressed as $P_{target} = [z_{target}, e_{target}, n_{target}]$. Finding the intersection point of a vector and a plan can be expressed as:

$$P_{int} = P_{start} + \frac{-(P_{start} - P_{target})N_{target}^T}{(P_{end} - P_{start})N_{target}^T}(P_{end} - P_{start}) \tag{2.29}$$

2.6 Error Propagation

Error propagation is the problem to find the distribution of a function with several random variables. There is no error propagation method be applied in heliostat field before. In other fields, error propagation is widely used. For example, mobile localization analysis, Error propagation for relative motion determined from marker positions etc. Leon Hall1 and Kristiaan Schreve(Page, 2010) using error propagation method to analysis an articulated arm. Arras, Ko(Arras and Arras, 1998) gives a introduction of error propagation derivation.
Error Propagation Law can be expressed as:

$$C_Y = F_X C_X F_X^T \tag{2.30}$$

Figure 2.15 shows a basic idea of one-dimensional case about error propagation problem. Variable X in the function $f(X)$ have uncertainties. Because this uncertainties transferred by function f, output Y should also have a uncertainties. By using Taylor series expansion, function f can be seen as a linear function. Then the uncertainties distribution could keep the same for X and Y.

For n-dimensional case, the output's parameter is expressed as:

$$\mu_Y = f(\mu_1, \mu_2, ..., \mu_n) \tag{2.31}$$

$$\sigma_Y \approx \sum_i^n (\frac{\partial f}{\partial X_i})^2 \sigma_i^2 \tag{2.32}$$

For n input two output, it can be expressed as:

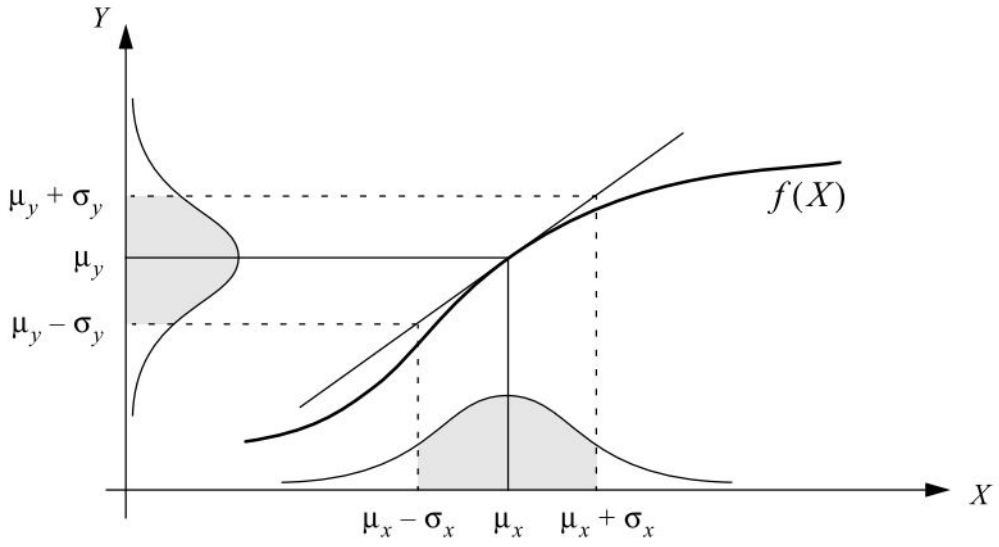

Figure 2.15: One-dimensional case of a nonlinear error propagation problem.(Arras and Arras, 1998)

$$\mu_Y = f_1(\mu_1, \mu_2, ..., \mu_n) \tag{2.33}$$

$$\sigma_Y^2 \approx \sum_i^n (\frac{\partial f_1}{\partial X_i})^2 \sigma_i^2 \tag{2.34}$$

$$\mu_Z = f_2(\mu_1, \mu_2, ..., \mu_n) \tag{2.35}$$

$$\sigma_Z^2 \approx \sum_i^n (\frac{\partial f_2}{\partial X_i})^2 \sigma_i^2 \tag{2.36}$$

$$\sigma_{YZ} = \sum \frac{\partial f_1}{\partial X_i} \frac{\partial f_2}{\partial X_i} \sigma_i^2 + \sum \sum_{i \neq j} \frac{\partial f_1}{\partial X_i} \frac{\partial f_2}{\partial X_j} \sigma_{ij}^2 \tag{2.37}$$

Chapter 3

Heliostat Error Model

The heliostat error model is a mathematical model that takes the heliostat errors as input parameters and gives the position of the reflected solar rays on the target plan as output. The heliostat error model used by Malan (2014) is also used here. The mathematical heliostat error model is implemented in Matlab code. This chapter validates the implemented code and gives some result from the heliostat error model.

3.1 Validation

In this section, the implementation of the solar vector is validated as well as the implementation of the heliostat error model.

3.1.1 Solar Vector

Solar vector is a unit direction vector point to the sun from a selected position on the earth. It gives the direction information from the selected position to the sun. While developing the model for solar vector, each step has been tested individually. The sun azimuth angle (γ_s) and the sun altitude angle (α_s) can be calculated with the calculator provided by Swinton (1920). This section compares the result of solar vector model with the online calculated result. In the error model, it uses one specific day's solar vector data to simulate. It shows the solar vector equations as following:

$$\hat{s} = s_e\hat{e} + s_n\hat{n} + s_z\hat{z} \tag{3.1}$$

where $s_e = \cos(\alpha_s)\sin(\gamma_s)$, $s_n = \cos(\alpha_s)\cos(\gamma_s)$, $s_z = \sin(\alpha_s)$

Moreover, because of the solar vector is based on the sun azimuth angle and the sun altitude angle, the validation process only compares the angle difference as Figure 3.1 shows.

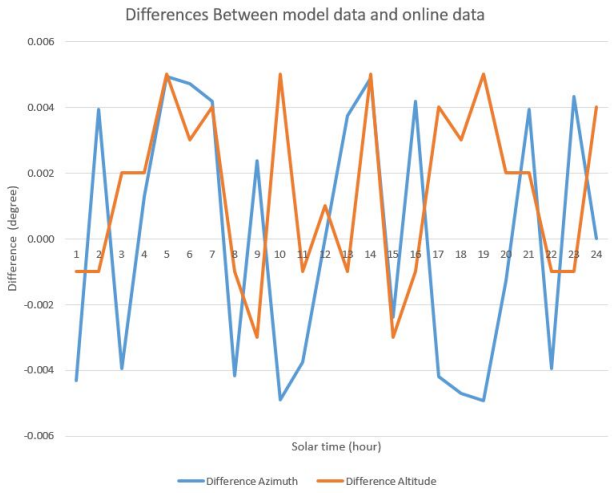

Figure 3.1: The result shows the different in 24 solar hours between angle calculated from the model and online calculator. It chooses 100 for day number and -33.936 degree for latitude.

The result shows that all angle differences are less than 0.006 degrees. That difference is caused by the accuracy level of implement model differ from the calculator. The error is small enough to conclude that the implemented model is correct. In the next section, this solar vector is used in the error model.

3.1.2 Error Model

In the error model, each step has been tested. Moreover, the heliostat error model was analyzed in the paper of Stone *et al.* (1995) then Malan (2014) validated his model with this heliostat error model. The implementation of the error model is validated by comparing results from it with results given in Malan (2014). Section 2.5 showed that the error model has 11 inputs for this model which are:

- Elevation angle offset error and azimuth angle offset error.
- North-south pedestal tilt error and east-west pedestal tilt error.
- Mirror alignment non-orthogonality errors.
- Three displacement errors.
- Location of target plane.

- Location of heliostat.
- Solar vector.

With those inputs are exactly known, the plot calculated from the model will have all the points at the origin, which means the reflected rays hit the central receiver exactly where it should, throughout the day.

The model uses the solar vector at date 21/12/2012 which means the day number is 355 and a latitude of 33.93 degree north. The heliostat is set at 50 m south of the tower, and the target is at the height of 13 m. The following figures show results on the target plane with different hours in a day. Because in the model, displacement errors directly affect the result on the target plane which does not need to be validated.. The model is validated with first three kinds of errors mentioned above. The figure is not exactly same because of the solar vector inputs for the model is nor exactly same with Malan (2014).

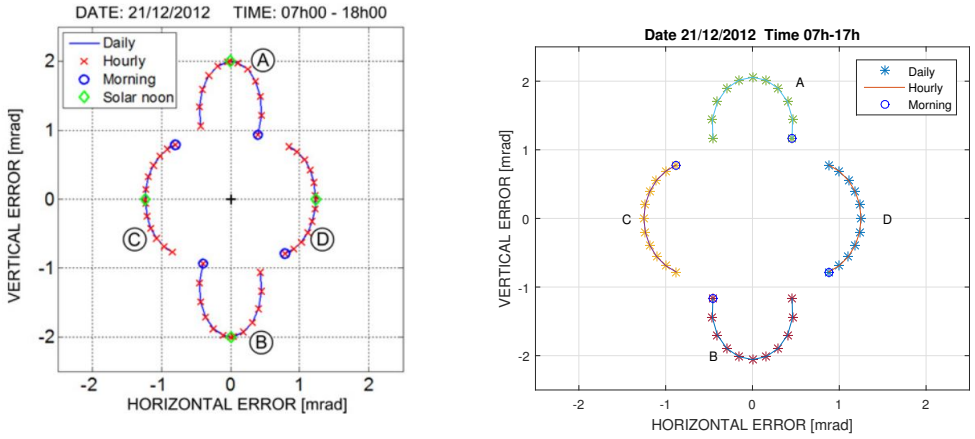

Figure 3.2: The model with errors for 1 mrad pedestal title toward (A)North, (B)South, (C)West and (D)East. The left figure is the result from Malan and the right one is from the model in this paper.

Figure 3.2 shows results from the model with pedestal tilt errors. Each point on the figure represents the reflected solar ray on the target plan at a specific solar time. The line in the figure represents the trajectory of reflected solar rays from time to time, and the points in the circle show the first reflected points on the target plane in that day. The pedestal of this heliostat is not perfect perpendicular to the ground, in this different figure lines means different 1 mard pedestal tilt angle in directions. The result shows how reflected solar rays looks like on the target plane. It can be seen that the shape of two consequence is almost same.

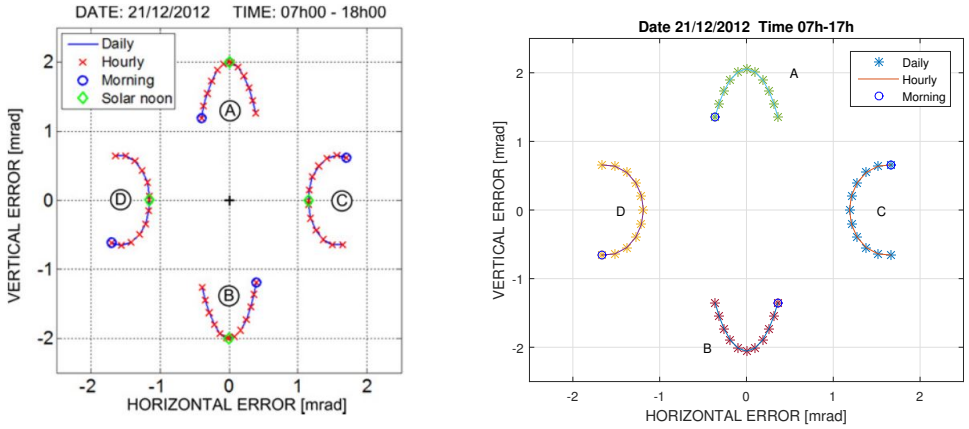

Figure 3.3: The model with errors for bias offset. (A)$\alpha_{bias} = 1$ mrad, (B)$\alpha_{bias} = -1$ mrad, (C)$\gamma_{bias} = 1$ mrad (D)$\gamma_{bias} = -1$ mrad. The left figure is the result from Malan and the right one is from the model in this paper.

Figure 3.3 shows the result with four different bias angle offset errors and elevation offset errors. Elevation offset error is the mirror plane of heliostat not perfect point to the expected direction. It is alignment canted due to different reasons. We can see that the shape of two results is similar.

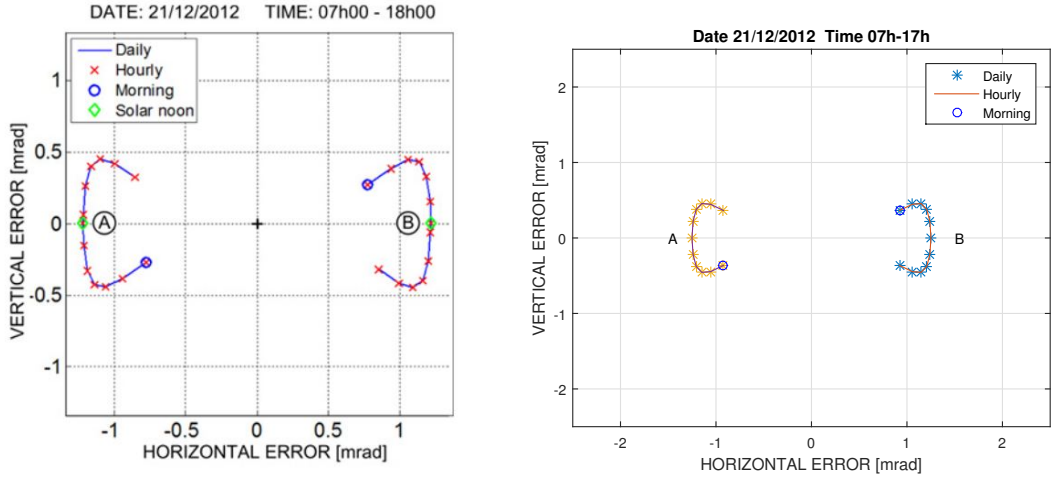

Figure 3.4: Non-orthogonality errors [mrad]: $\varepsilon_{no} = 1$ and $\varepsilon_{no} = -1$. Result from Karel (left) and result from model(right)

Figure 3.4 shows non-orthogonal errors. This error makes the pedestal of heliostat has a rotation for 1 mard around the pedestal. The results is similar.

3.2 Result from the heliostat error model

After built the error model, the result of the heliostat error shows how date and solar time affect the consequence on reflected image. And with the position of heliostat changed result also changed accordingly. In this section, it will illustrate different date and positions of heliostat affect the result throughout a day.

3.2.1 Effect of date and time

In this section, the effect of the data and time on the reflected solar rays is considered for different errors in the heliostat model. The location of heliostat for tracking result is same as previous one $(1, 0, -50)$,(Z,E,N) and target is 13 meters high. Solar vector is tested on five different day numbers: $1, 101, 201, 250, 301$.

3.2.1.1 Solar vector effect on Pedestal Error

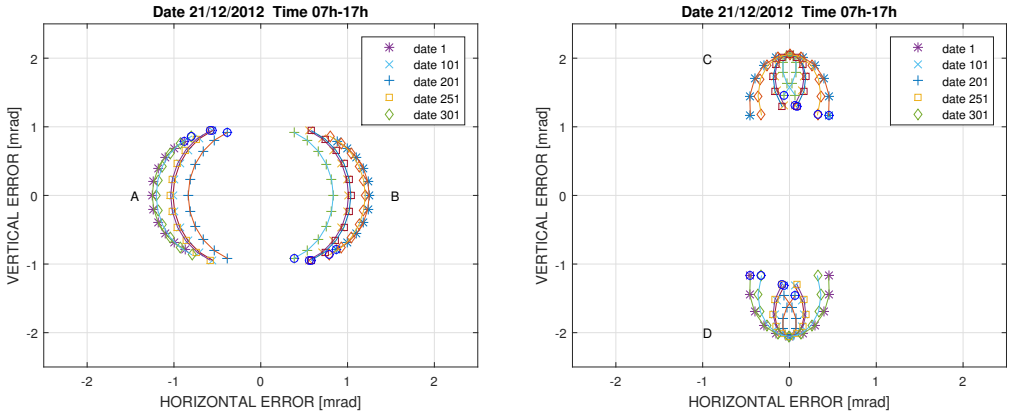

Figure 3.5: Pedestal tilt errors with different solar vector. The model with errors for 1 mrad pedestal title toward (A)West and (B)East (left), (C)North and (D)South (right). In the figure it shows 5 different solar vectors from different time.

Figure 3.5 shows the result with Pedestal tilt errors $\varepsilon_{ptn} = 1$ mrad (left) and $\varepsilon_{pte} = 1$ mrad (right) in five different solar vectors with different time. The figures clearly show that as time change, the trajectory of the reflected rays' position on the target can be far away from the center. In the left figure, we can see that with time changes, reflected points' trajectory was moving closer to the center as date number increasing from 1 to 201. After date 201, reflected points goes back to the same position as date 1. In the right figure,

it shows the trajectory close from date 1 to date 201 and then open again.

3.2.1.2 Solar vector effect on the combination of bias offset errors

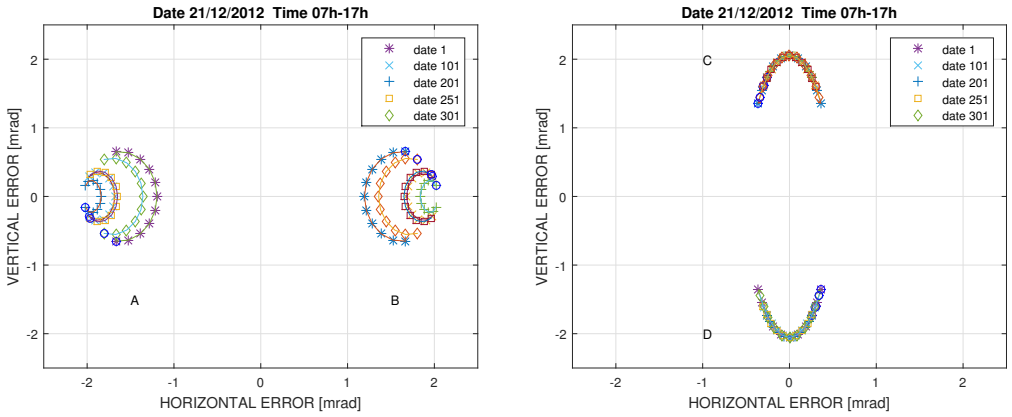

Figure 3.6: Bias offset errors with different solar vector. The model with errors for 1 mrad azimuth bias(A)West, (B)East (left) and 1 mrad elevation bias (C)North, (D)South (right). In the figure it shows 5 different solar vectors from different time.

Figure 3.6 shows the result with all the heliostat errors zero except the azimuth bias angle $\gamma_{bias} = 1$ mard(left) and elevation bias angle $\alpha_{bias} = 1$ mard(right). It can be seen that in the left figure, the trajectory of reflected points goes away from central with the date from day 1 to day 200. After that it goes back again as date number increasing to the end of the year. However, elevation bias has no affect on the trajectory with the date changed all the year.

3.2.1.3 Solar vector effect on Non-Orthogonality Error

The tracking result shows in Figure 3.7, and it can be seen that the distance from reflected points to the central is becoming smaller with the increasing of date number.After the 200th day of a year, the reflected points goes away from the central point again. At the first day in a year, reflected point has almost the largest distance from central points, while, at the 200th day in a year, the distance becomes almost smallest. After that, the distance increases back as the begin of the year.

All the previous figures indicate that the date and time of a year do affect the tracking result of the heliostat error model. The exactly trajectory of reflected solar rays on the target with the different date is dependents on the

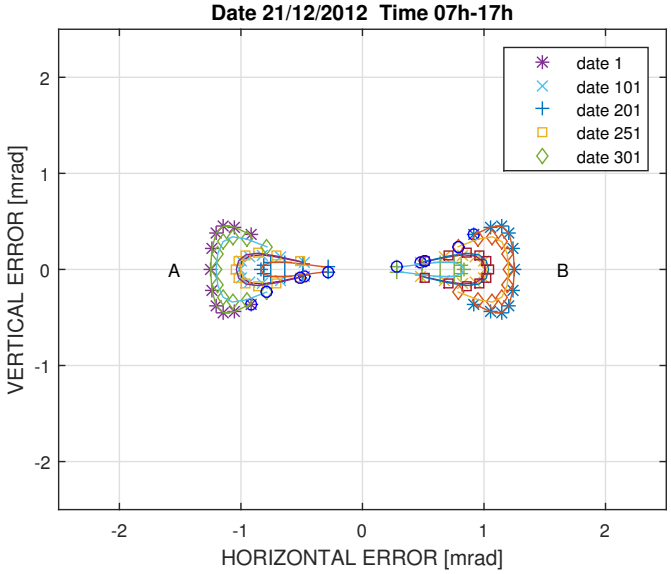

Figure 3.7: Non-Orthogonality error with solar vectors in five different days. (A):$\varepsilon_{no} = -1$, (B):$\varepsilon_{no} = 1$.

individual heliostat errors. Using a well-calibrated heliostat model is important. Otherwise, the reflected solar rays may far of the target.

3.2.2 Effect of the heliostat position

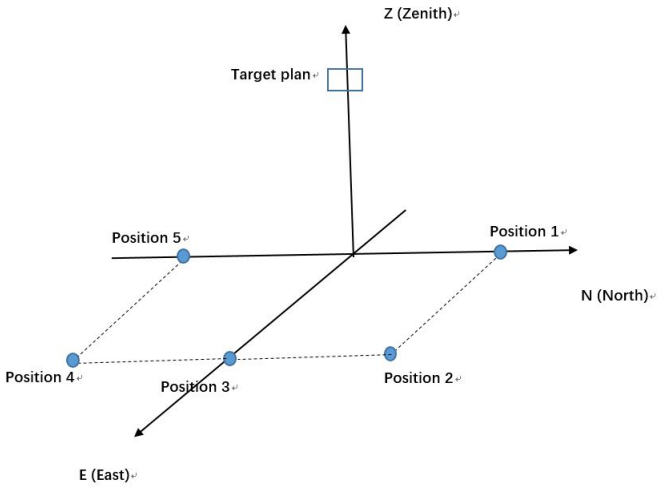

Figure 3.8: Five different positions for Heliostats

This section discusses the tracking result for a different position of a heliostat. The solar vector is for day number 355, the target is 13 meters high.

Figure 3.8 gives five different position where heliostats is placed at. Those five different positions(Z,E,N) are arranged clockwise :$(1, 0, 50)$ north of the tower, $(1, 50, 50)$ north-east of the tower, $(1, 50, 0)$ east of the tower, $(1, 50, -50)$ east-south of the tower , $(1, 0, 50)$ south of the tower.

3.2.2.1 Different heliostats with pedestal errors

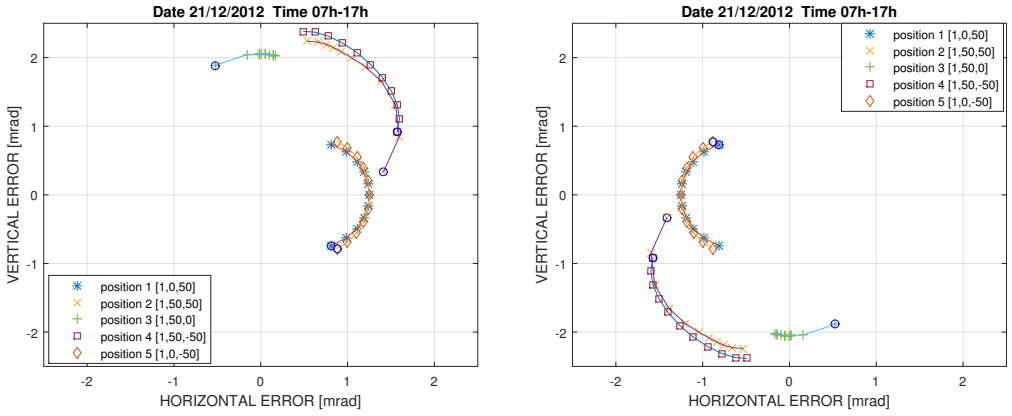

Figure 3.9: Pedestal tilt errors with different heliostat. The model with errors for 1 mrad pedestal title toward East(left) and West(right) shows five results with each heliostat.

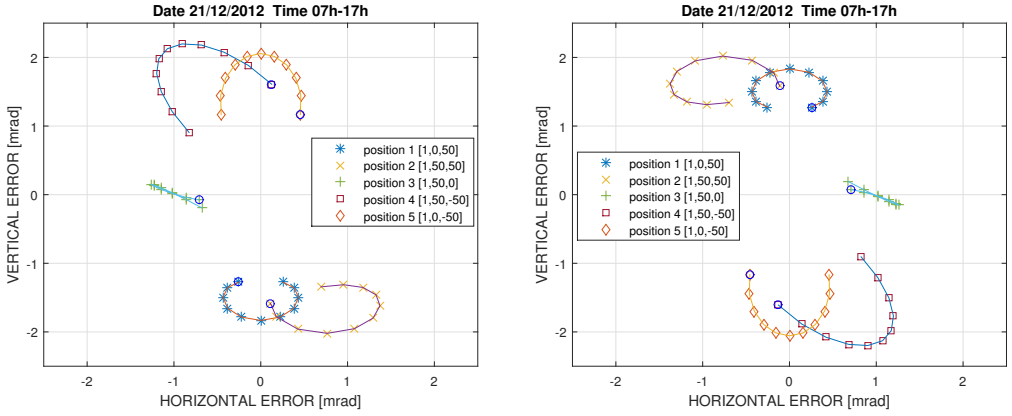

Figure 3.10: Pedestal tilt errors with different heliostat. The model with errors for 1 mrad pedestal title toward North(left) and South(right) shows five results with each heliostat.

Figure 3.9 shows the result with all the heliostat errors zero except pedestal tilt errors $\varepsilon_{pte} = \pm 1$ mrad. The points with different shapes refer to different heliostat tracking result. It clearly shows that with position changed, the shape of error tracking result also changed. With the target plan faced to East, the heliostat's result is symmetric with East-axis which means heliostat at position 1 and 5 have similar result and position 2 and 4 have similar result.

Figure 3.10 shows the result with all the heliostat errors zero except pedestal tilt errors $\varepsilon_{ptn} = \pm 1$ mrad. It also shows that the result is related to heliostat position. When the position of heliostat symmetric with East-axis, the consequence on the target plan is also symmetric with central point.

3.2.2.2 Different heliostats with bias offset errors

After setting five heilostat positions, Figure 3.11 shows the result with all the heliostat azimuth bias angle are $\gamma_{bias} = \pm 1$ mard. With the errors, the result become complex. It can be seen that the shape of error tracking result is changed a lot with different heliostat positions.

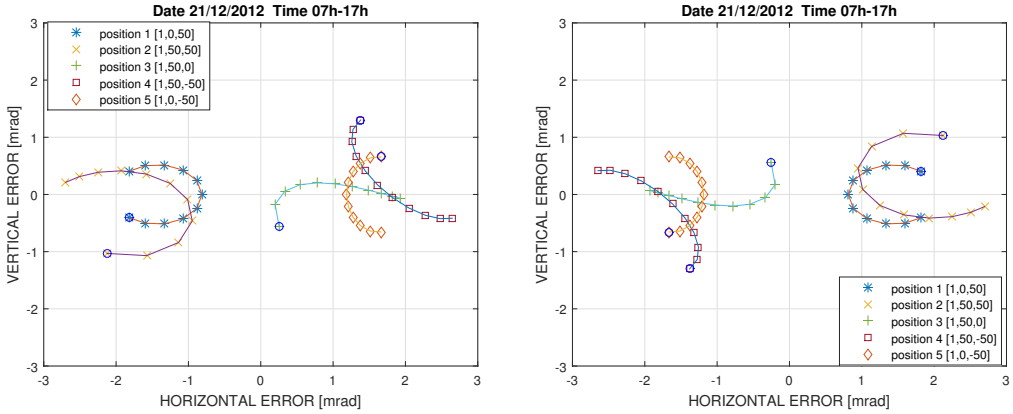

Figure 3.11: Bias offset errors with different heliostat position. The model with title azimuth bias $\gamma_{bias} = 1$ mrad (left) and $\gamma_{bias} = -1$ mrad (right) shows five results with each heliostat.

Figure 3.12 shows the result with all the heliostat elevation bias angle are $\alpha_{bias} = \pm 1$ mard. With the errors. It can be seen that the shape of error tracking result is changed by heliostat positions.

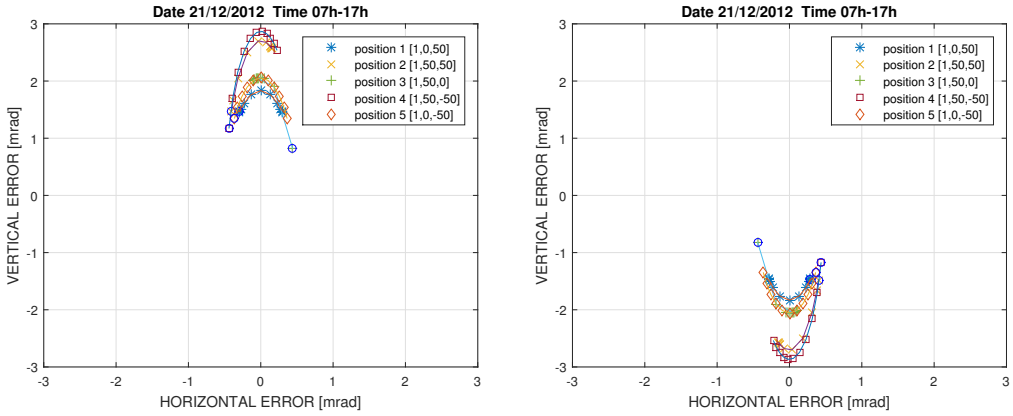

Figure 3.12: Bias offset errors with different heliostat position. The model with title elevation bias $\alpha_{bias} = 1$ mrad (left) and $\alpha_{bias} = -1$ mrad (right) shows five results with each heliostat.

3.2.2.3 Different heliostats with non-orthogonality error

Figure 3.13 shows the results with non-orthogonality error $\varepsilon_{no} = \pm 1$ mrad with different heliostat positions. It can be seen that the shape of result is changed with different heliostats.

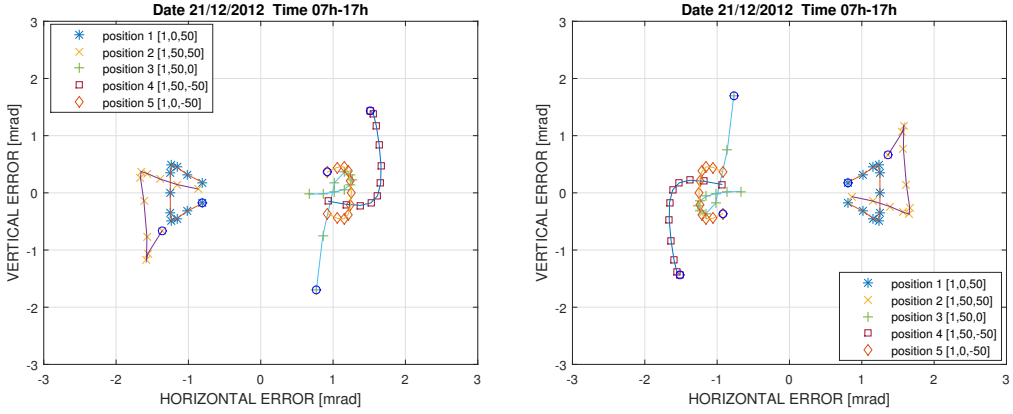

Figure 3.13: Non-orthogonality error with different heliostats. $\varepsilon_{no} = -1$ mrad (left). $\varepsilon_{no} = 1$ mrad (right)

Different heliostat positions change the reflected points' trajectory as Figure 3.9 to 3.13 shows. The position of heliostat have different affection on different errors. Normally the reflected points have a symmetry relationship based on heliostat position.

In generally, for a particularly reflected point, the results dependent on every parameter inputs in the model. Which means it is difficult for a system to trace back the accuracy errors' value simply by error model.

The next chapter discusses the error propagation model, which is used to analyze the tracking result for heliostat errors that are not exactly known, like in this chapter, but that are known only to certain degree.

Chapter 4

Error Propagation Model

Chapter 3 discussed the effect of the solar vector and the position of the heliostat about the tower on the reflected solar rays on the target plane.

In this chapter, the error propagation law is applied to the heliostat error model, and the result is called the error propagation model which is first derived. After that, the derivation is validated by comparing the result distribution from derived model with the consequence from Monte Carlo simulation. As we apply first-order Taylor series expansion in error propagation if the heliostat error function is too far from linear, the approximation of consequence can be poor. At the other hand, we can expect the consequence of error propagation model is close enough to the result from Monte Carlo simulation. At last, some result from the derived model is discussed.

4.1 Model Derivation

The error propagation model is finding the distribution of outputs from a function with several random input variables. Which means we are going to figure out the first two statistical moments, that is the mean $\mu_{outputs}$ and the second (central) moment $\sigma^2_{outputs}$, the variance. Normally we have the distribution of inputs.

For the heliostat error model, it means that uncertainties in the errors of the heliostat will cause uncertainties in the position of the reflected rays on the target. In this case, there are eight uncertainty inputs and two uncertainty outputs. As Figure 4.1 shows, the model produces the coordinates of the reflected points on target plan. Here follows the application of the error propagation law on the heliostat error model.

Figure 4.1 shows the error propagation model system. In this case, it has eight

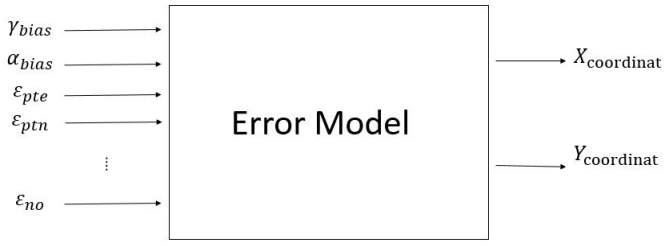

Figure 4.1: Error Propagation Model Of Heliostat

error inputs, and two outputs:

Each error is assumed to have a standard normal distribution. The errors' distribution can be differ due to different environment. In this case, we are assume errors with the mean equal to 0 mrad and the variance equal to 1 mrad^2.

$$Error_i \sim N(\mu_i, \sigma_i^2) \tag{4.1}$$

Where $\mu_i = 0$ mrad, $\sigma_i^2 = 1$ mrad^2

The error propagation equation can be expressed as:

$$C_{xy} = F_{input} C_{input} F_{input}^T \tag{4.2}$$

Where C_{xy} is 2×2 output covariance matrix. F_{input} is Jacobian matrix. The diagonal of covariance matrix is the variance of errors along X and Y axes.

$$C_{xy} = \begin{bmatrix} \sigma_x^2 & \sigma_x\sigma_y \\ \sigma_x\sigma_y & \sigma_y^2 \end{bmatrix} \tag{4.3}$$

Since there are eight inputs, the 8×8 input covaricance matrix can be express as:

$$C_{input} = \begin{bmatrix} \sigma_{e1}^2 & \sigma_{e1e2} & \cdots & \sigma_{e1e8} \\ \sigma_{e2e1} & \sigma_{e2}^2 & \cdots & \sigma_{e2e8} \\ \vdots & \vdots & \ddots & \vdots \\ \sigma_{e8e1} & \sigma_{e8e2} & \cdots & \sigma_{e8}^2 \end{bmatrix} \tag{4.4}$$

The Jacobian Matrix F can be shown as:

$$F_{input} = \begin{bmatrix} \dfrac{\partial F_X}{\partial e_1} & \cdots & \dfrac{\partial F_X}{\partial e_8} \\ \dfrac{\partial F_Y}{\partial e_1} & \cdots & \dfrac{\partial F_Y}{\partial e_8} \end{bmatrix} \tag{4.5}$$

To combine all matrix together, by equation 4.2, the Error Propagation Model

can be expressed as:

$$\begin{bmatrix} \sigma_x^2 & \sigma_x\sigma_y \\ \sigma_x\sigma_y & \sigma_y^2 \end{bmatrix} =$$

$$\begin{bmatrix} \frac{\partial F_X}{\partial e_1} & \cdots & \frac{\partial F_X}{\partial e_8} \\ \frac{\partial F_Y}{\partial e_1} & \cdots & \frac{\partial F_Y}{\partial e_8} \end{bmatrix} \begin{bmatrix} \sigma_{e1}^2 & \sigma_{e1e2} & \cdots & \sigma_{e1e8} \\ \sigma_{e2e1} & \sigma_{e2}^2 & \cdots & \sigma_{e2e8} \\ \vdots & \vdots & \ddots & \vdots \\ \sigma_{e8e1} & \sigma_{e8e2} & \cdots & \sigma_{e8}^2 \end{bmatrix} \begin{bmatrix} \frac{\partial F_X}{\partial e_1} & \frac{\partial F_Y}{\partial e_1} \\ \vdots & \vdots \\ \frac{\partial F_X}{\partial e_8} & \frac{\partial F_Y}{\partial e_8} \end{bmatrix} \tag{4.6}$$

In order to find out distribution of outputs we can calculate the mean of results which is :

$$\begin{aligned} \mu_x &= F_x(\mu_1, \mu_2, \cdots, \mu_8) \\ \mu_y &= F_y(\mu_1, \mu_2, \cdots, \mu_8) \end{aligned} \tag{4.7}$$

4.2 Error Propagation Model Result

Each inputs parameters has an effect on the result of reflected points distribution. For the following results, we choose the solar vector of day 355 and heliostat with coordinate $(1, 0, -50)$ to keep the same with previous chapters. The result shows three different solar times on the same day. With all errors' distribution are assumed to be normal distribution with $\mu_i = 0$ mrad, $\sigma_i^2 = 1$ mrad^2, the result covariance matrix shows as following:

$$Cxy = \begin{bmatrix} 404.384 & 0.000 \\ 0.000 & 408.461 \end{bmatrix} \tag{4.8}$$

Where the variation of x,y coordinate for the point on the target plan are:

$$\begin{aligned} \sigma_x^2 &= 404.384 \quad & mrad^2 \\ \sigma_y^2 &= 408.461 \quad & mrad^2 \end{aligned} \tag{4.9}$$

$$\begin{aligned} \mu_x &= 0 \quad & mrad \\ \mu_y &= 0 \quad & mrad \end{aligned} \tag{4.10}$$

Setting all errors to zero, the result of error propagation model illustrate that at solar noon, reflected sunlight rays reaching the target plan with a wider errors distribution along the x-axis and more narrow distribution along the y-axis. Along x-axis, the reflected points have a Gaussian distribution with mean equal to 0 and variance equal to 1.011. Along y-axis, the reflected points have a Gaussian distribution with mean equal to 0 and variance equal to 0.102.

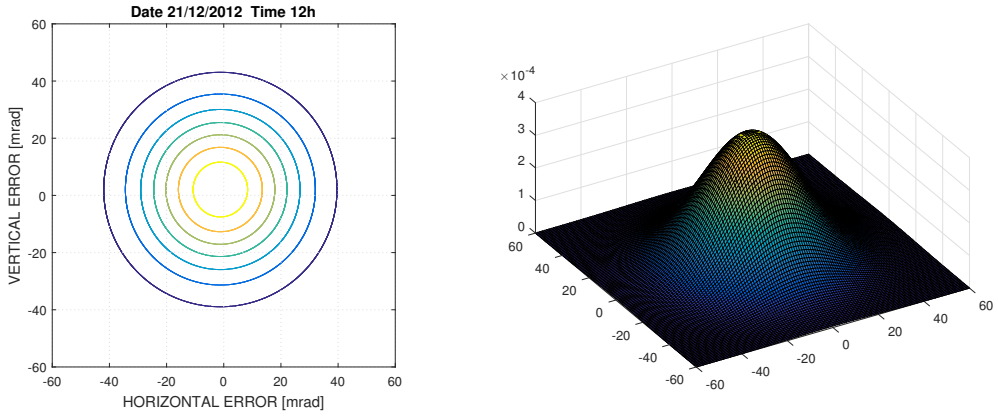

Figure 4.2: Distribution of reflect points on the target plan.

As Chapter 3.2.1 shows, we will give more results with changing parameters. Solar time, the different date also has an effect on the error propagation results. Figure 4.3 shows results with different solar time and different date though a year.

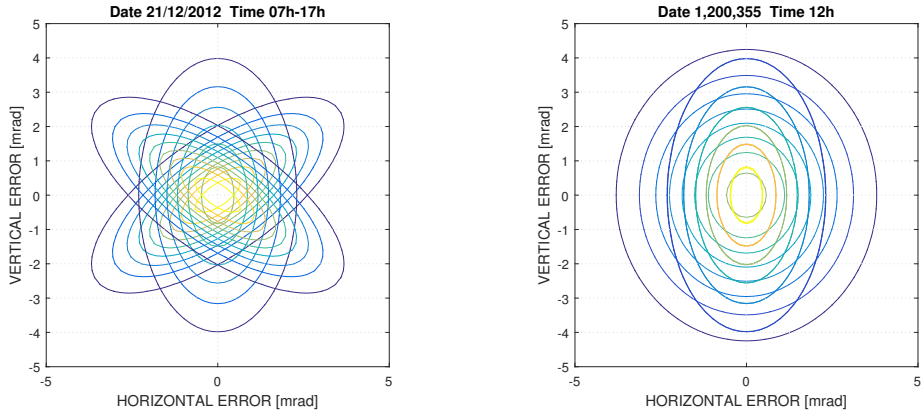

Figure 4.3: Distribution of reflect points on the target plan. Assuming pedestal errors has a normal distribution mean equal to 0 and variance equal to 1. Left: Different solar time though one day. Right: Different date with same solar time though one year.

Figure 4.4 gives a results with different heliostat positions. We choose three heliostat positions here $[1, 0, 50], [1, 50, 0], [1, 0, -50]$ comparing with Chapter 3.2.2. The figure is symmetry when pedestal errors change to opposite value.

After validated, we will apply error propagation model on some questions in chapter 5 and at that time, we will show distribution figures.

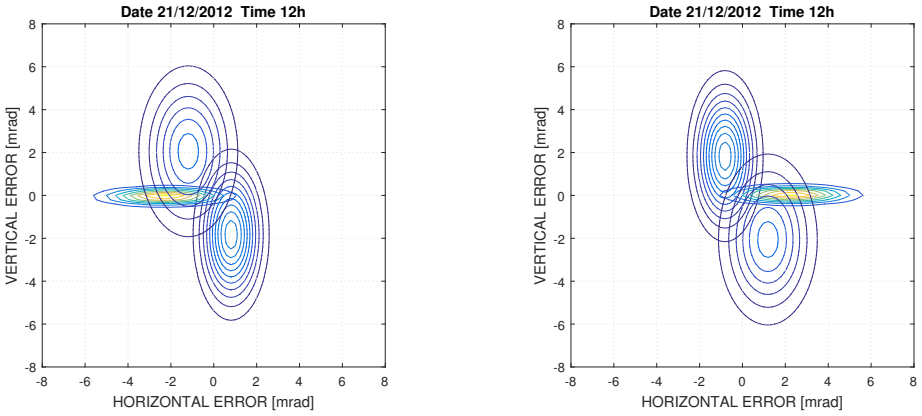

Figure 4.4: Distribution of reflect points on the target plan. Assuming pedestal errors has a normal distribution which variance equal to 1. The figure shows 3 different heliostat positions. Left: pedestal title errors' mean equal to -1. Right: pedestal title errors' mean equal to 1.

4.3 Validation

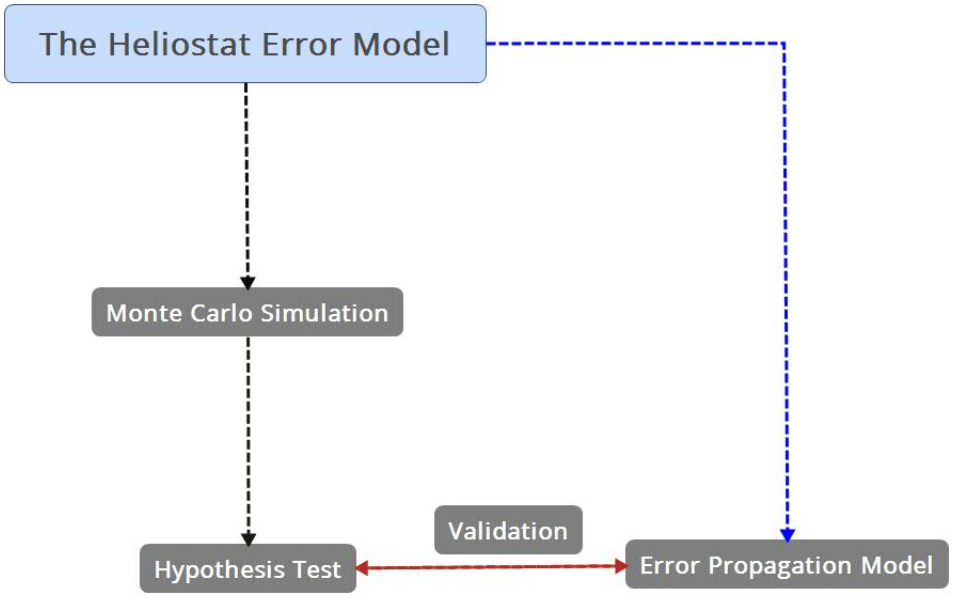

Figure 4.5: First uses a Mote Carlo simulation to generate samples which can be used in hypothesis testing to comparing with the results from error propagation model.

This section validates the implementation of the error propagation model. First, it uses a Monte Carlo simulation to generate samples from the heliostat error model which has already been validated. Then it uses hypothesis

testing to check if the results from the error propagation model are correct by comparing it to the results from the Monte Carlo simulation. We set same error parameters to both error propagation model and Monte Carlo model and check if Monte Carlo simulation's result can be seen as generated from error propagation model. Figure 4.5 shows the validation flow.

4.3.1 Monte Carlo Simulation

The Monte Carlo method is a computational method. The principle is that by giving a large number of random samples to the model to obtain numerical results. Using large random sampling to understand a system and simulate the system.

This Monte Carlo simulation uses repeated random sampling to generate simulated data that shows the relationship between inputs and outputs. In general, there are four steps to apply to a Monte Carlo Simulation. For validation purposes, the solar vector corresponding to day 355 at $12:00$ is used, the heliostat is at position $(1, 0, -50)$ which is keeping the same with previous chapter.

Step 1. Identify an appropriate mathematical model for the Monte Carlo simulation. In this case, the validated heliostat error model is used.

Step 2. Define the inputs and outputs of the mathematical model in step 1.
Each error is assumed to be a normal distribution with zero mean and standard deviation at one. The solar vector, the positions of the heliostat and the position of the target not changed. For outputs, the model gives the coordinates of the reflected points on the target plan.

Step 3. Create random input data
As the parameters defined, it is simple to create valuable for each error input using the function "normrnd$(0, 1)$" in Matlab.

Step 4. Simulate and analyze outputs with the random input data.
Running a large enough number of simulations, the Monte Carlo simulation will lead to reliable outputs to do the analysis. In this case, the simulation was run $10,0000$ times.

We set the same error parameters as error propagation model in Figure 4.2, and the Monte Carlo model distribution result shows on the target plane as Figure 4.6. It can be seen that the distribution of errors along the Y-axis is similar with errors along X-axis. In addition, the distribution of errors along both axes seems to have the same mean 0. This distribution result is similar to

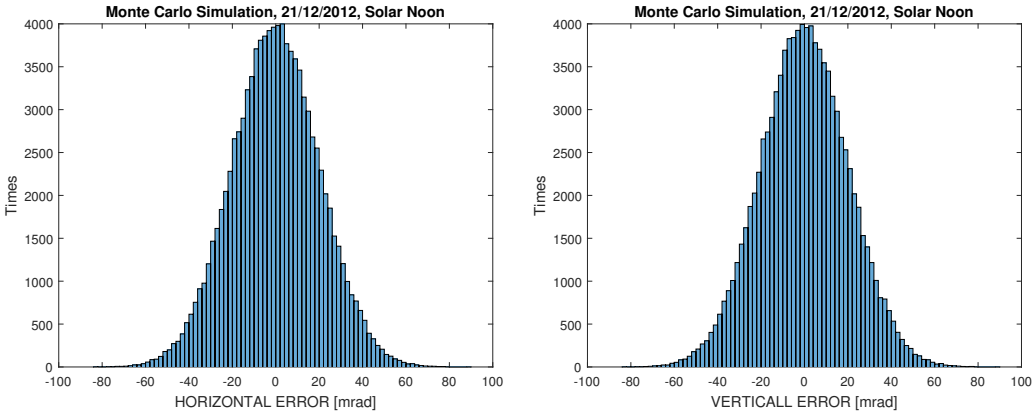

Figure 4.6: Monte Carlo simulation result of the error model with the result from the error propagation model superimposed.

the result of the error propagation model, and they would be compared more precisely in the next section.

4.3.2 Hypothesis Testing

A hypothesis is a statement about the population parameters to be tested, such as population mean, variance, etc. A hypothesis test is used to determine if there is enough evidence in the data to support the hypothesis based on statistics and probability theory. It has two opposing hypothesis to be tested in the theory, null hypothesis and alternative hypothesis. Based on the data, the test determines whether to reject the null hypothesis or not. We use p-value to determine the consequence. If the p-value is less than or equal to a specific value, we can reject the null hypothesis. Otherwise, we can not reject the hypothesis.

This section gives the validation of the error propagation model by comparing its results with the Monte Carlo simulation results. Hypothesis testing use statistics to determine the probability that a given hypothesis is true. Normally, the process of hypothesis testing consists of four steps as Figure 4.7 shows:

Step 1: Between the result from Monte Carlo Simulation and Error Propagation Model, there are two components should be compared to, the mean (μ_x and μ_y) of errors and the variance (σ_x^2 and σ_y^2) of errors. The null hypothesis can be set as:

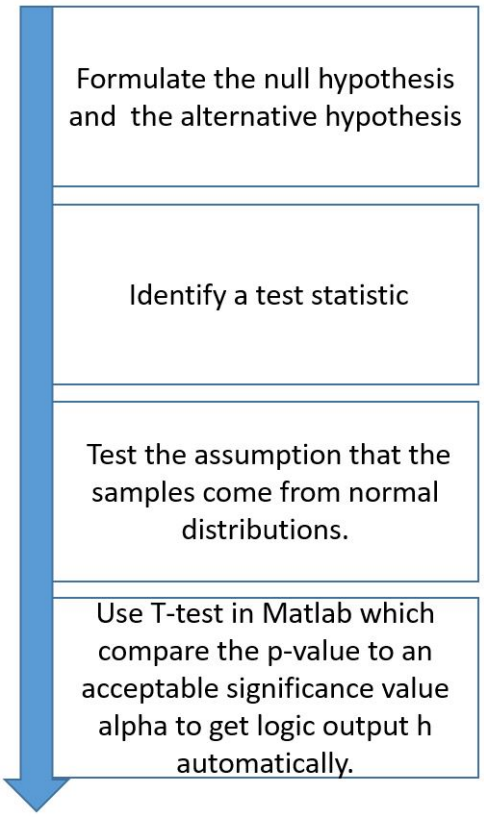

Figure 4.7: Hypothesis Testing Process

$$\begin{aligned} H_o^1 &: \mu_x = 0 \\ H_o^2 &: \mu_y = 0 \\ H_o^3 &: \sigma_x^2 = 404.384 \\ H_o^4 &: \sigma_y^2 = 408.461 \end{aligned} \tag{4.11}$$

Then the alternative hypothesis becomes:

$$\begin{aligned} H_a^1 &: \mu_x \neq 0 \\ H_a^2 &: \mu_y \neq 0 \\ H_a^3 &: \sigma_x^2 \neq 404.384 \\ H_a^4 &: \sigma_y^2 \neq 408.461 \end{aligned} \tag{4.12}$$

Step 2: In this part, to check the hypothesis relating to mean values, it uses T-test statistic, and Chi-square test statistic is used to check hypothesis relating to variance values.

Step 3: Test the assumption that the samples generated from Monte Carlo simulation are come from a normal distribution. Figure 4.8 shows that all

data is along a straight line, which means that all data are come from normal distribution.

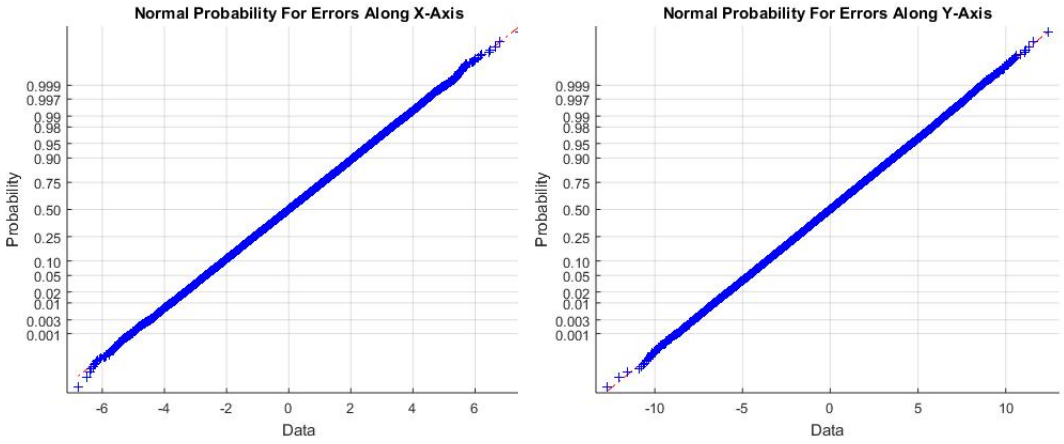

Figure 4.8: A normal probability plot of errors along x-axis and y-axis

Table 4.1: Hypothesis Test Result

Hypothesis	H	P-Value	Test Stastic	Matlab Test Function
1	0	0.3073	T-test	ttest
2	0	0.1602	T-test	ttest
3	0	0.5387	Chi-square test	vartest
4	0	0.9717	Chi-square test	vartest

Step 4: Table 4.1 shows the result of Hypothesis Test. First two hypothesis prove that the data from Monte Carlo simulation has a zero mean. Moreover, last two hypothesis test prove that the data has the same variance with error propagation model result. Value H in the table is a logic result generated from the Matlab function which indicates if the null hypothesis can be rejected or not. In the result, it shows H for all hypothesis are equal to 0 which means the test can not reject the null hypothesis. The mean and variance of sample data are same as error propagation model result. The smaller P-value is, the more doubt of there is in the validity of a null hypothesis. Only hypothesis two has a relatively low P-value, but this value is still large enough to accept the hypothesis.

4.4 Conclusion

As hypothesis test proved, with all error has a normal distribution in the model, error propagation model obtain the same reflected points distribution as Monte Carlo simulation. It shows heliostat error model is linear enough to be used in error propagation law and the result from error propagation model is acceptable.

The error propagation model is derived base on the heliostat error model mentioned in Chapter 2. Eight errors are included in this model, and there may have more sources of errors exist in other error models. Some errors can be combined with one error source and others cannot. In this error propagation model, it only shows the error effect of those eight errors and gives the distribution of points on the target plane. With this error propagation model, some questions about the heliostat error model can be answered, such as how sensitive the result is to various heliostat error parameters. The application of error propagation model will be discussed in next chapter.

Chapter 5

Results

The error propagation model has been validated in the last chapter. It is now used to answer some questions about the effect of calibration errors in the heliostat model on the control accuracy of the heliostat. Each question is briefly described and some results are shown at the end of each section. All questions are tested with the heliostat at position $(1, 0, -50)$, the target plant at a height of 13 meters, and a solar vector on day $355th$.

5.1 Pedestal Tilt

Central receiver plant are usually built in dry areas. However, after heavy rains in such area, the ground of some heliostats may be changed which will slant the heliostat in some direction. If this new slant is not accounted for in the heliostat model, it will result in an error which will affect the control accuracy. How does this slant affect the heliostat's reflection on the target plane.

5.1.1 Method

Figure 5.1 shows a heliostat slanted in some direction. The slant angle is θ_{bias}. This slant causes pedestal tilt and it can be separated into two pedestal tilt errors, a counter-clockwise rotation error around the E-axis (ε_{pte}) and a counter-clockwise rotation error around the N-axis (ε_{ptn}). Several scenarios are tested. Each scenario assumes a certain error in the calibraion model, given by $\mu_{\varepsilon_{pte}}$, $\mu_{\varepsilon_{ptn}}$ and σ^2_{error}. The distribution of the reflected rays on the target is presented at different times of the day, namely 7h, 9h, 12h, 15h and 17h.

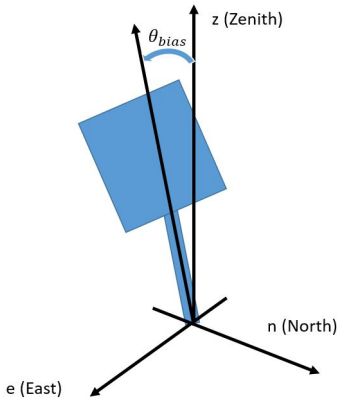

Figure 5.1: Heliostat slant due to rain.

5.1.2 Result

Figure 5.2 to Figure 5.5 shows the distribution of the reflected rays on the target, for different errors in the pedestal tilt. Take Figure 5.2 as an example, with $\mu_{\varepsilon_{pte}} = 1$ mrad, $\mu_{\varepsilon_{ptn}} = 1$ mrad and $\sigma^2_{error} = 1$ mrad^2. The reflected rays will generally be focused to the top-left of the target. In all four figures, the distribution of the reflected rays moves counter-clockwise as the day progresses.

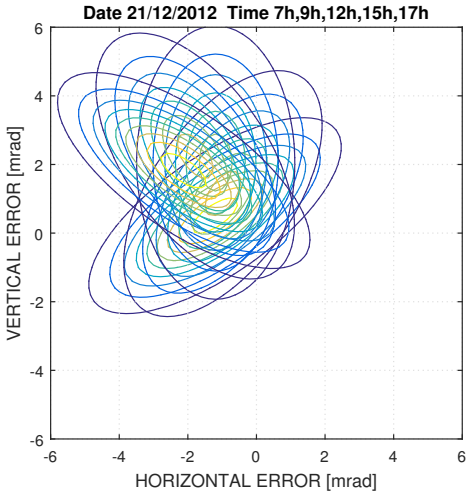

Figure 5.2: Distribution of errors along x-axis and y-axis with heliostat slant with $\mu_{\varepsilon_{ptn}} = 1$ mrad, $\mu_{\varepsilon_{pte}} = 1$ mrad and $\sigma^2_{error} = 1$ mrad^2

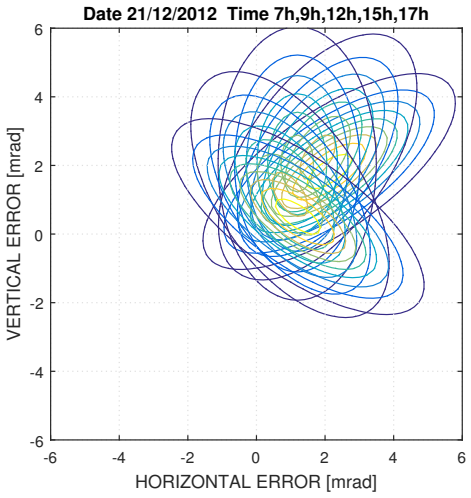

Figure 5.3: Distribution of errors along x-axis and y-axis with heliostat slant with $\mu_{\varepsilon_{ptn}} = 1$ mrad, $\mu_{\varepsilon_{pte}} = -1$ mrad and $\sigma^2_{error} = 1$ mrad^2

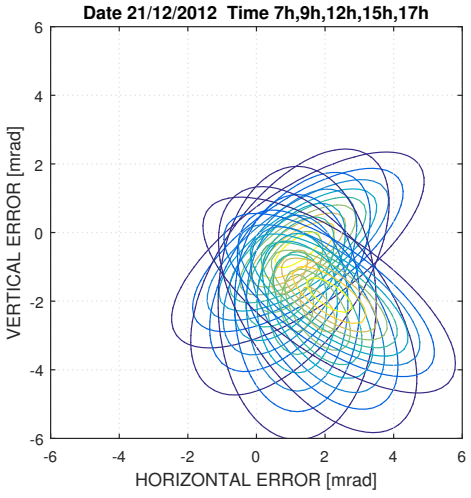

Figure 5.4: Distribution of errors along x-axis and y-axis with heliostat slant with $\mu_{\varepsilon_{ptn}} = -1$ mrad, $\mu_{\varepsilon_{pte}} = -1$ mrad and $\sigma^2_{error} = 1$ mrad^2

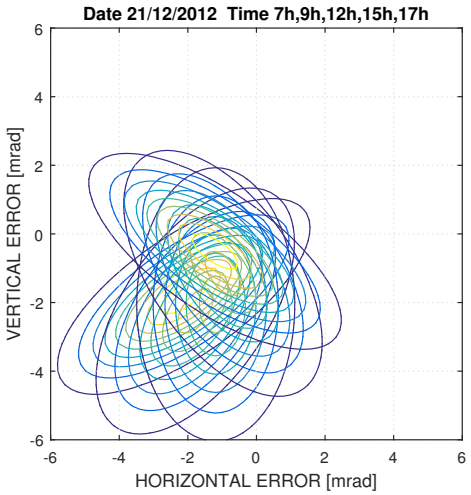

Figure 5.5: Distribution of errors along x-axis and y-axis with heliostat slant with $\mu_{\varepsilon_{ptn}} = -1$ mrad, $\mu_{\varepsilon_{pte}} = 1$ mrad and $\sigma^2_{error} = 1$ mrad^2

5.2 Required Measurement Accuracy

How accurate could the position of the reflected rays on the target plane be found?

5.2.1 Method

Different combination of errors can result in a different distribution of points on the target plane. Besides, the distribution range for errors also affect the reflected rays on the target plan. The way to solve this problem is first to estimate the errors that remain on the heliostat after calibration process. After that, set errors' distribution and use the error propagation model to see how it affects the accuracy on the target plane. In this question, we assume an error distribution with $\sigma^2_{error} = 1$ mrad^2 and $mean = 0$ mrad to each error which make the result easier to understand. The result shows the accuracy to where the position of the reflected rays has to be measured, in order to get a calibration result for a control accuracy of 1 mrad. We choose solar noon and a heliostat at $[1, 0, -50]$ as default parameter.

5.2.2 Result

In this result, as we assume the mean of errors equal to zero so that reflected rays will distribute around the center on the target plan. So we only focus on the variance distribution of the reflected rays. First, we use Figure 5.6 shows the result of all errors remaining on the heliostat, each of them has a normal

distribution. We get a distribution with $\sigma_x^2 = 404.38$ mrad^2 $\sigma_y^2 = 408.46$ mrad^2 and $mean = 0$ mrad

- Pedestal tilt North (mrad)
- Pedestal tilt East(mrad)
- Axes Non-Orthogonality (mrad)
- Bias angle (mrad)
- Heliostat(B) Location translation (m)
- Heliostat(B) Location translatrion (m)
- Heliostat(B) Location translation (m)

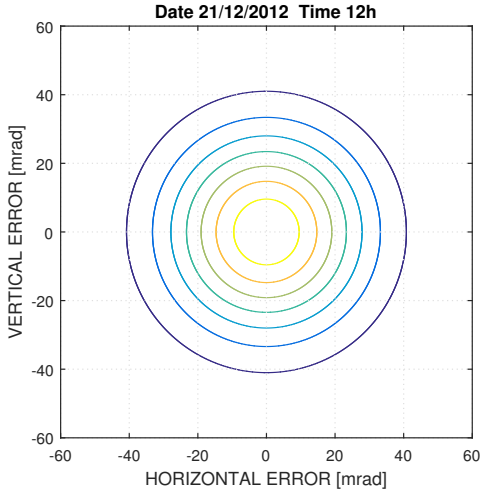

Figure 5.6: Result distribution along X-axis and Y-axis with all errors

In another Example, Figure 5.7 shows result of three mainly errors remaining on the heliostat and each of them has a normal distribution $\sigma_{error}^2 = 1$ mrad^2 and $mean = 0$ mrad. We have a distribution for reflected points with $\sigma_x^2 = 4.384$ mrad^2 $\sigma_y^2 = 8.461$ mrad^2 and $mean = 0$ mrad

- Azimuth bias angle (mrad)
- Elevation bias angle (mrad)
- Axes Non-Orthogonality (mrad)

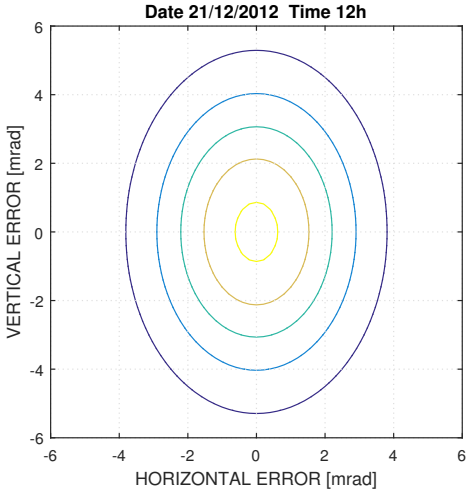

Figure 5.7: Result distribution along X-axis and Y-axis with three kinds of errors.

In next Example, Figure 5.8 shows the result of three kinds of errors as following, remaining on the heliostat and each of them has a normal distribution $\sigma^2_{error} = 1$ mrad^2 and $mean = 0$ mrad. We have a distribution for reflected points with $\sigma^2_x = 400$ mrad^2 $\sigma^2_y = 400$ mrad^2 and $mean = 0$ mrad. The huge reflected rays' distribution is because of the error have large distribution range which is unit counting by meter.

- Heliostat(B) Location translation (m)
- Heliostat(B) Location translatrion (m)
- Heliostat(B) Location translation (m)

5.3 Error Sensitivity

What is the sensitivity of each error? Which error has the biggest affect on the reflected rays for a heliostat?

5.3.1 Method

Different combination of errors can result in a different distribution of points on the target plane. Errors in this specific heliostat($[1, 0, -50]$) will be tested one by one at solar noon. Besides, the result of the test will show the sensitive of each error. In this case, each error has a normal distribution as before, and the result will be compared to figure out effect from different error.

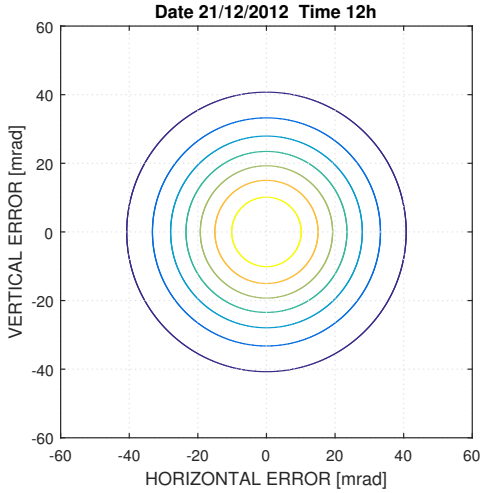

Figure 5.8: Result distribution along X-axis and Y-axis with three kinds of errors.

5.3.2 Result

Table 5.1: Error affect on reflected rays

Error type	Mean of result	Variance of result along X-axis	Variance of result along Y-axis
ε_{pte}	0	0.000	4.230
ε_{ptn}	0	1.409	0.000
ε_{no}	0	1.566	0.000
γ_{bias}	0	1.409	0.000
α_{bias}	0	0.000	4.230
D_z	0	0.000	378.21
D_e	0	400.0	0.000
D_n	0	0.000	21.785

Table 5.1 shows the effect of each error. It illustrates that for this heliostat ($[1, 0, -50]$), pedestal tilt towards e-axis ε_{pte} and elevation bias α_{bias} have the biggest effect on reflected rays along Y-axis direction, mirror alignment non-orthogonality errors ε_{no} has the biggest effect on reflected rays along X-axis direction. Heliostat position offsets do have a huge effect on reflected rays, but it is due to the different unit. Eight kinds of errors show as below:

- Pedestal tilt towards e-axis ε_{pte} (mrad)
- Pedestal tilt towards n-axis ε_{ptn} (mrad)
- Mirror alignment non-orthogonality errors ε_{no} (mrad)

- Azimuth bias γ_{bias} (mrad)
- Elevation bias α_{bias} (mrad)
- Heliostat(B) Location translation D_z(m)
- Heliostat(B) Location translatrion D_e(m)
- Heliostat(B) Location translation D_n(m)

5.4 Effect of Solar Vector

How does the solar vector affect reflected rays with different errors for a heliostat?

5.4.1 Method

For this question, using different days solar vector with error combinations can illustrate the effect of solar vectors. The result will show a distribution of reflected rays, and it will use the same heliostat($[1, 0, -50]$) as before. Solar vector is tested on nine different days in a year $(1, 46, 91, 136, 181, 226, 271, 316, 361)$. And the result shows the effect of the solar vector on different errors and a combination of eight errors.

5.4.2 Result

1. Figure 5.9 shows that the variance of North pedestal tilt error does not change with different solar vector during a year. The top yellow points show errors' variance along Y-axis, and the bottom blue points show errors' variance along X-axis. Both of them unchanged during the year.

2. Figure 5.10 gives the result for the variance of East pedestal tilt error changed with different solar vector during a year. The variance for two distributions changed at the beginning, mid and end of a year. The blue points at top show errors' variance along X-axis it has the highest value at around mid of the year.

3. Figure 5.11 shows the effect of a combination of bias offset errors with different solar vector during a year. The variance of result along x-axis does not have a significant change during a year, while, the result variance along y-axis has a minimum value at mid of the year and a higher value at beginning and end of the year.

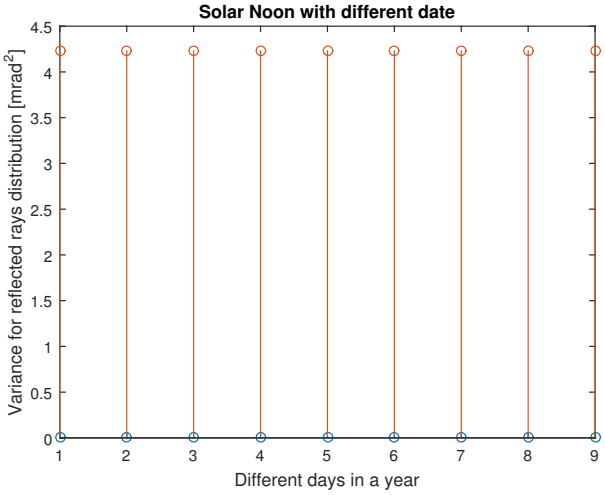

Figure 5.9: Result variances along X-axis and Y-axis during a year with north pedestal tilt error

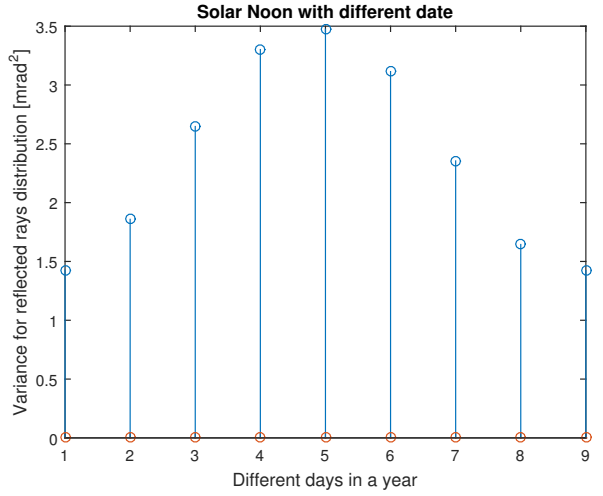

Figure 5.10: Result variances along X-axis and Y-axis during a year with east pedestal tilt error

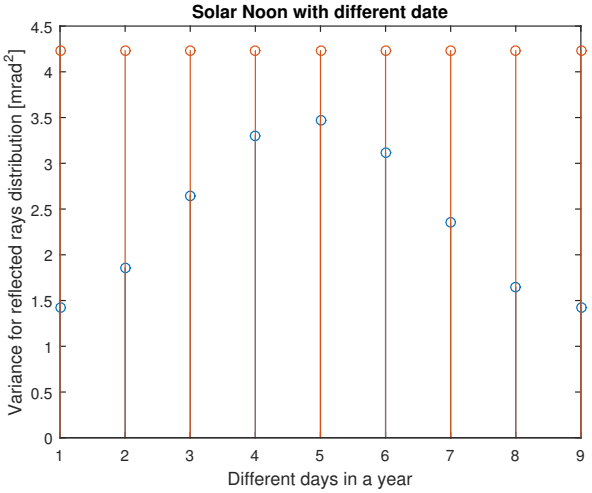

Figure 5.11: Result variances along X-axis and Y-axis during a year with bias offset errors

4. Figure 5.12 illustrates the effect by a non-orthogonality offset error with different solar vector during a year. The distribution variance of result along x-axis keeps zero through a year, and the distribution variance along y-axis has a minimum value at mid of the year and a higher value at beginning and end of the year.

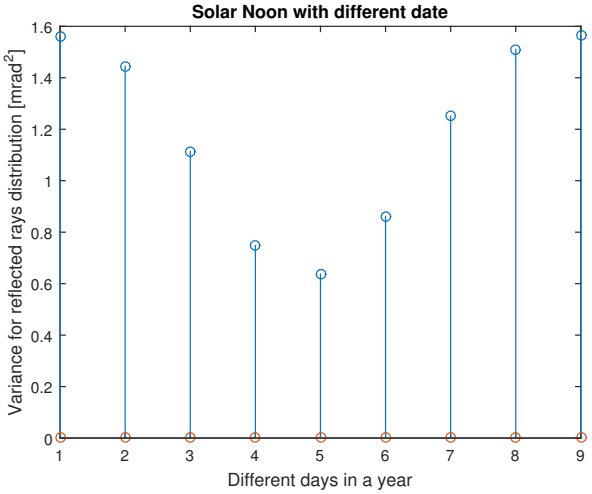

Figure 5.12: Result variances along X-axis and Y-axis during a year with a non-orthogonality offset errors

5. Figure 5.13 illustrates the effect by a combination of five mainly errors during a year. Distribution variance along x-axis keeps same during the year

while, the distribution variance along y-axis arrive the biggest value at the mid of the year.

- Pedestal tilt towards e-axis ε_{pte} (mrad)
- Pedestal tilt towards n-axis ε_{ptn} (mrad)
- Mirror alignment non-orthogonality errors ε_{no} (mrad)
- Azimuth bias γ_{bias} (mrad)
- Elevation bias α_{bias} (mrad)

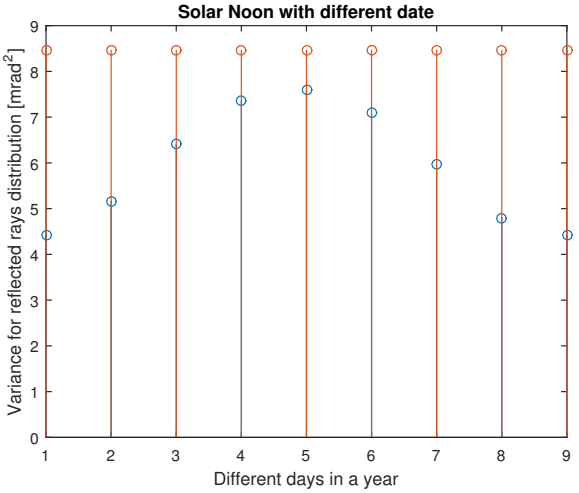

Figure 5.13: Result variances along X-axis and Y-axis during a year with combination of five mainly errors

The result shows that the solar vector has a different effect on the reflected rays only on variance distribution along the y-axis. The results show the variance distribution along y-axis fluctuates with the solar vector which looks similar to the trigonometric function.

5.5 Effect of Heliostat Position

How does the position affect reflected rays with different errors?

5.5.1 Method

As mentioned in Chapter 3.2.2, it uses different heliostat positions to calculate the result of reflected rays distributed. After that, by comparing the variance and means, it can show how the position of heliostat affect the reflected rays. We choose solar noon and the 355th day of a year. The heliostat is selected in five different positions:
$(1, 0, 50), (1, 50, 50), (1, 50, 0), (1, 50, -50), (1, 0, -50)$.

5.5.2 Result

Figure 5.14 gives the result of reflected rays' distribution for different heliostats with pedestal title errors. The positions of heliostats has effect on the result as following figure shows.

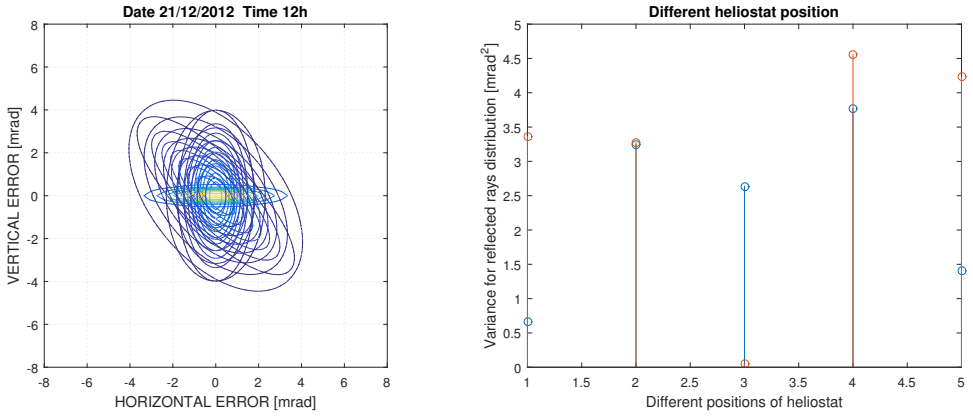

Figure 5.14: Pedestal title errors with different heliostat position reflected rays. The distribution variances along X-axis and Y-axis with different heliostats. Left: Contour figure for reflected rays distribution. Right: Reflected rays distribution variance.

For bias angle γ_{bias} and α_{bias}, heliostat position also change the reflected ray's distribution variance as Figure 5.15 shows.

With all eight errors, the distribution can be changed a lot by heliostat location changed. With the high distribution variance of heliostat location translation errors, it is hard to see the result changes in Figure 5.16. So we ignore the heliostat location translation errors to see what happens.

With all eight errors except heliostat location translation, the distribution of reflected ray changes obviously. Figure 5.17 gives reflected rays' distribution

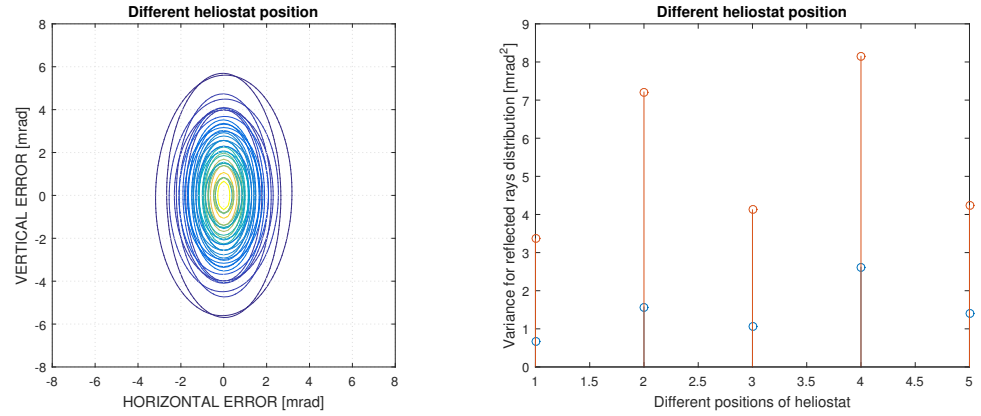

Figure 5.15: Bias angle errors with different heliostat position reflected rays. The distribution variances along X-axis and Y-axis with different heliostats. Left: Contour figure for reflected rays distribution. Right: Reflected rays distribution variance.

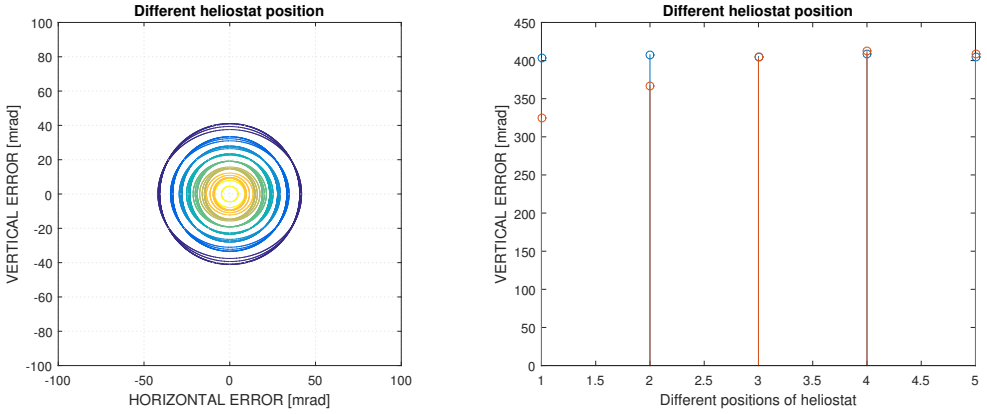

Figure 5.16: All errors with different heliostat position reflected rays. The distribution variances along X-axis and Y-axis with different heliostats. Left: Contour figure for reflected rays distribution. Right: Reflected rays distribution variance.

and their variance distribution. With the position of heliostat changes, reflected ray also has a different distribution.

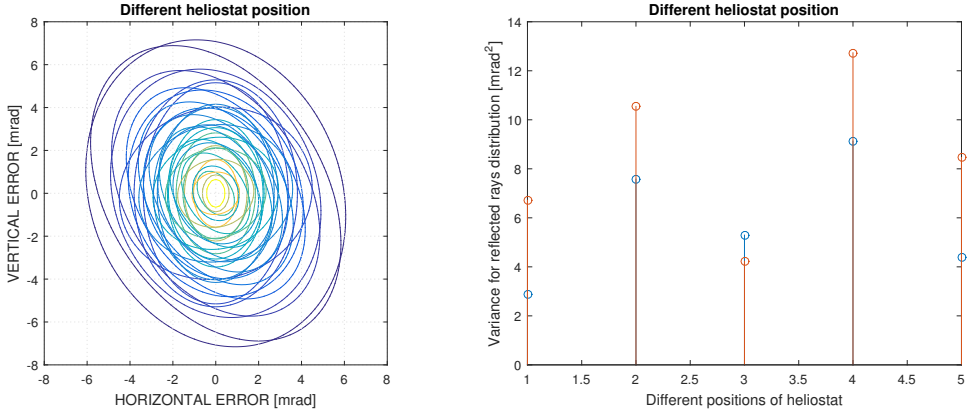

Figure 5.17: All errors except heliostat translation with different heliostat position reflected rays. The distribution variances along X-axis and Y-axis with different heliostats. Left: Contour figure for reflected rays distribution. Right: Reflected rays distribution variance. Variance distribution along X-axis is bigger than that along Y-axis except the third heliostat.

Chapter 6

Conclusions

This paper is focused on getting a better understanding of the helisotat error model by using an error propagation model. This chapter summarize the research in this thesis. First section summarize the main work in the research while the math conclusions are discussed in section 6.2. Finally section 6.3 gives some suggestion for possible future work.

6.1 Summary of the work

The research conducted in this thesis was motivated by the demand of the analysis of heliostat control accuracy. Several errors exist in the heliostat model which increase the complexity of heliostat calibration. For fixed errors in a heliostat, the reflected rays' distribution on target plan is helpful to the calibration process.

A heliostat error model is established according to the work of Malan (2014). A solar vector model is established (Swinton, 1920) which provide solar information to the heliostat error model. Solar vectors were used to calculate reflected rays from the heliostat error model.

An error propagation law is applied to the heliostat error model.

The research uses a Monte Carlo Method to validate the heliostat error propagation model.

6.2 Conclusions

The research objectives have been met. The heliostat error propagation model presented here can also be used to solve other questions related to the effect

of calibration errors.

6.3 Suggestions for future work

The error model derived with the error propagation law can be used to investigate various aspects related to heliostat calibration and control accuracy. There are possible directions for future research in:

- Validate the accuracy of the heliostat error model based against a real heliostat mechanism system. The system could also include more errors such as air refraction, a curved mirror, etc.
- Design a new type of heliostat calibration algorithm, based on results from error propagation model.

Appendices

Appendix A

Model Validation Results

The validation has been done in Chapter 3. Here gives other 3 figures comparing the result between implementation error heliostat model and Malan (2014). The heliostat position is $[1, 30.8, -19.2]$.

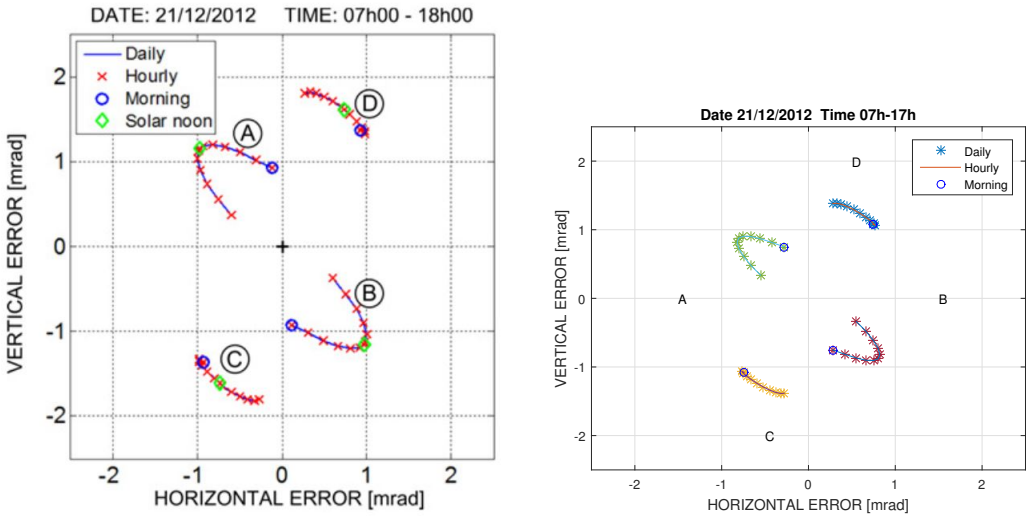

Figure A.1: The model with errors for 1 mrad pedestal title toward (A)North, (B)South, (C)West and (D)East. The left figure is the result from Malan and the right one is from the model in this paper.

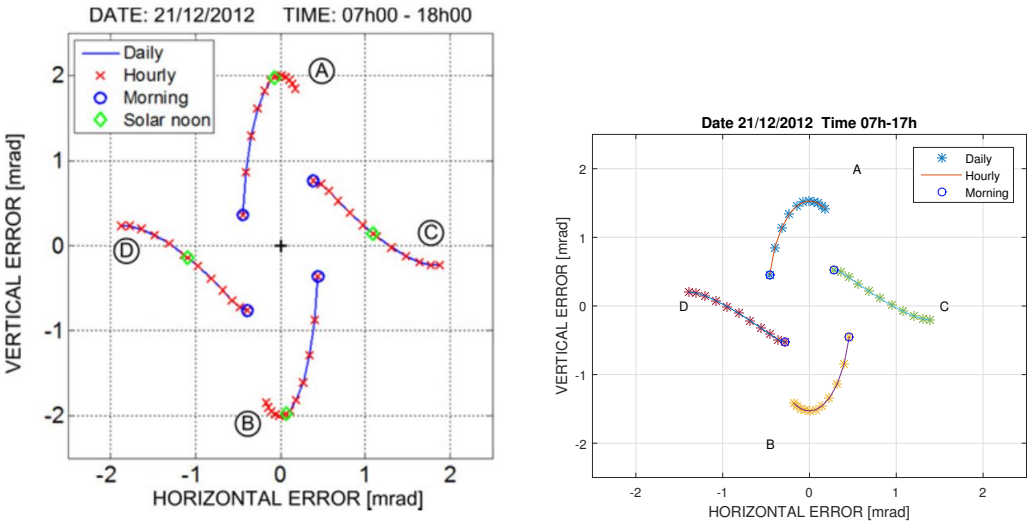

Figure A.2: The model with errors for bias offset. (A)$\alpha_{bias} = 1mrad$, (B)$\alpha_{bias} = -1mrad$, (C)$\gamma_{bias} = 1mrad$ (D)$\gamma_{bias} = -1mrad$. The left figure is the result from Malan and the right one is from the model in this paper.

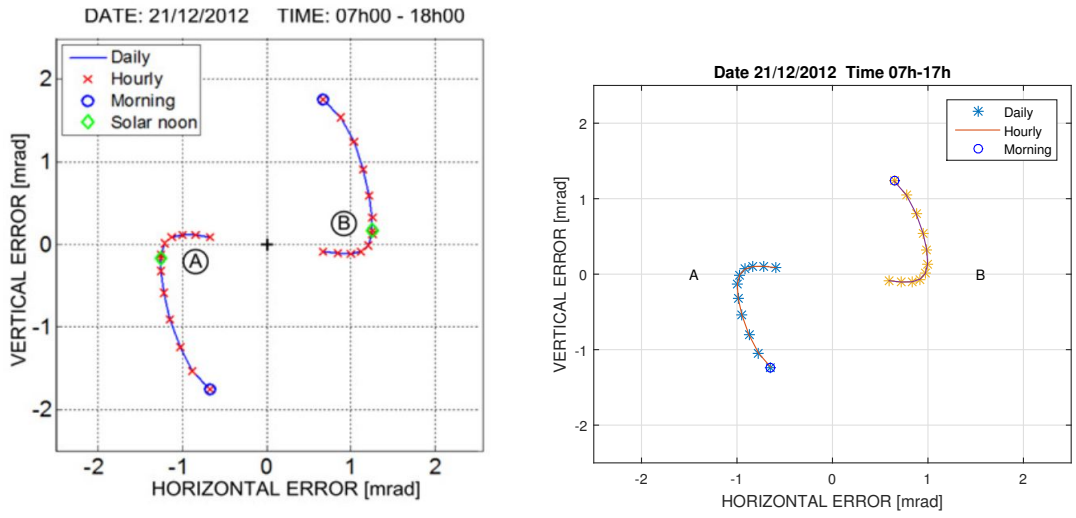

Figure A.3: Non-orthogonality errors [mrad]: $\varepsilon_{no} = 1$ and $\varepsilon_{no} = -1$. Result from Karel (left) and result from model(right)

List of References

Abengoa (). Abengoa About Atacama-1 Images.
Available at: http://www.abengoa.com/web/en/novedades/atacama-1/acerca/imagenes/

Aiuchi, K., Yoshida, K., Onozaki, M., Katayama, Y., Nakamura, M. and Nakamura, K. (2006). Sensor-controlled heliostat with an equatorial mount. *Sol. Energy*, vol. 80, pp. 1089–1097. ISSN 0038092X.

Arras, K. and Arras, K. (1998). An Introduction to Error Propagation: Derivation, Meaning, and Examples of Equation cy= fx cx fx. *Lausanne Swiss Fed. Inst. Technol. Lausanne*, , no. September, pp. 98–01.
Available at: http://scholar.google.com/scholar?hl=en&btnG=Search&q=intitle:An+Introducti

Baheti, R. and Scott, P. (1980). Design of self-calibrating controllers for heliostats in a solar power plant. *IEEE Trans. Automat. Contr.*, vol. 25, no. 6, pp. 1091–1097. ISSN 0018-9286.
Available at: http://ieeexplore.ieee.org/xpls/abs_all.jsp?arnumber=1102527

Behar, O., Khellaf, A. and Mohammedi, K. (2013). A review of studies on central receiver solar thermal power plants. *Renew. Sustain. Energy Rev.*, vol. 23, no. November 2015, pp. 12–39. ISSN 13640321.
Available at: http://dx.doi.org/10.1016/j.rser.2013.02.017

Berenguel, M., Rubio, F.R., Valverde, a., Lara, P.J., Arahal, M.R., Camacho, E.F. and López, M. (2004 jan). An artificial vision-based control system for automatic heliostat positioning offset correction in a central receiver solar power plant. *Sol. Energy*, vol. 76, no. 5, pp. 563–575. ISSN 0038092X.
Available at: http://linkinghub.elsevier.com/retrieve/pii/S0038092X0300464X

Chen, Y.T., Kribus, a., Lim, B.H., Lim, C.S., Chong, K.K., Karni, J., Buck, R., Pfahl, a. and Bligh, T.P. (2004). Comparison of Two Sun Tracking Methods in the Application of a Heliostat Field. *J. Sol. Energy Eng.*, vol. 126, no. 1, p. 638. ISSN 01996231.
Available at: http://solarenergyengineering.asmedigitalcollection.asme.org/article.aspx?a

Clifford, M.J. and Eastwood, D. (2004). Design of a novel passive solar tracker. *Sol. Energy*, vol. 77, no. 3, pp. 269–280. ISSN 0038092X.

Edition, F. (2012). Guide for Writing Technical Reports Guide for Writing Technical Reports.

Freeman, J. (2014). Study of the errors influencing heliostats for calibration and control system design. *Int. Conf. Recent Adv. Innov. Eng.*, pp. 1–8.
Available at: `http://ieeexplore.ieee.org/lpdocs/epic03/wrapper.htm?arnumber=6909113`

Gallego, B., Cohen, G., Mancini, T., Wilkins, T., Morse, F. and Kearney, D. (2012). The history of American CSP - A timeline.
Available at: `http://www.csptoday.com/usa/pdf/USAtimeline.pdf`

Hoffschmidt, B., Alexopoulos, S., Rau, C., Sattler, J., Anthrakidis, a., Boura, C., Connor, B.O. and Hilger, P. (2012). Concentrating Solar Power. *Compr. Renew. Energy*, vol. 3, no. 2, pp. 595–636. ISSN 0094243X.
Available at: `http://dx.doi.org/10.1016/B978-0-08-087872-0.00319-X`

Hogan, R., Pye, J., Ho, C. and Smith, E. (2013). Uncertainty analysis of heliostat alignment at the Sandia Solar Field. *Energy Procedia*, vol. 49, no. 1980, pp. 2100–2108. ISSN 18766102.
Available at: `http://linkinghub.elsevier.com/retrieve/pii/S1876610214006766`

Kearney, D. (2014). Utility-scale Power Tower Solar Systems: Performance Acceptance Test Guidelines. *Energy Procedia*, vol. 49, no. March, pp. 1784–1791. ISSN 1876-6102.
Available at: `http://www.sciencedirect.com/science/article/pii/S1876610214006432`

Kolb, G.J., Jones, S.a., Donnelly, M.W., Gorman, D., Thomas, R., Davenport, R. and Lumia, R. (2007). Heliostat Cost Reduction Study. *Test*, vol. SAND2007-3, no. June, pp. 1–158.
Available at: `http://www.osti.gov/bridge/product.biblio.jsp?query_id=1&page=0&osti_id=912`

Kribus, A., Vishnevetsky, I., Yogev, A. and Rubinov, T. (2004). Closed loop control of heliostats. *Energy*, vol. 29, no. 5-6, pp. 905–913. ISSN 03605442.
Available at: `http://linkinghub.elsevier.com/retrieve/pii/S0360544203001956`

Lee, C.-Y., Chou, P.-C., Chiang, C.-M. and Lin, C.-F. (2009 jan). Sun Tracking Systems: A Review. *Sensors*, vol. 9, no. 5, pp. 3875–3890. ISSN 1424-8220.
Available at: `http://www.pubmedcentral.nih.gov/articlerender.fcgi?artid=3297124&tool=pmce`

M. (2006); Pidwirny (). "Earth-Sun Geometry". Fundamentals of Physical Geography, 2nd Edition.
Available at: `http://www.physicalgeography.net/fundamentals/6h.html`

Malan, K.J. (2014). A Heliostat Field Control System. , no. March.
Available at: `http://scholar.sun.ac.za/handle/10019.1/86674`

Mousazadeh, H., Keyhani, A., Javadi, A., Mobli, H., Abrinia, K. and Sharifi, A. (2009). A review of principle and sun-tracking methods for maximizing solar systems output. *Renew. Sustain. Energy Rev.*, vol. 13, no. 8, pp. 1800–1818. ISSN 13640321.
Available at: `http://linkinghub.elsevier.com/retrieve/pii/S1364032109000318`

Müller-Steinhagen, H. and Trieb, F. (2004). Concentrating solar power - A review of the technology. *Q. R. Acad. Eng.*, pp. 43–50. ISSN 1095-9203.

Page, H. (2010). Error Distribution of an Articulated Arm Measurement System. , no. July, pp. 13–16.

Plant, G.C.R.C. (). High performance corrosion resistant tubing for solar power plant from Fine Tubes | Fine Tubes.
Available at: `http://www.finetubes.co.uk/case-studies/gemasolar-the-worlds-first-commerci`

Poulek, V. and Libra, M. (1998). New solar tracker. *Sol. Energy Mater. Sol. Cells*, vol. 51, no. 2, pp. 113–120. ISSN 09270248.

Ren21 (2015). RENEWABLES 2015 GLOBAL STATUS REPORT. pp. 1–33.
Available at: `http://www.ren21.net/wp-content/uploads/2015/07/GSR2015_KeyFindings_lowres.`

Rizk, J. and Chaiko, Y. (2008). Solar Tracking System: More Efficient Use of Solar Panels. *Proc. World Acad. Sci. Eng. Technol.*, vol. 43, pp. 313–315.

Rubio, F.R., Ortega, M.G., Gordillo, F. and López-Martínez, M. (2007). Application of new control strategy for sun tracking. *Energy Convers. Manag.*, vol. 48, no. 7, pp. 2174–2184. ISSN 01968904.

Stone, K.W., Beach, H. and Jones, S.a. (1995). Analysis of solar two heliostat tracking error sources. p. 10.
Available at: `http://www.osti.gov/scitech/biblio/20030576`

Swinton, a.a.C. (1920). Power from the Sun.
Available at: `http://www.powerfromthesun.net/Book/chapter03/chapter03.html`

Ulmer, S., März, T., Prahl, C., Reinalter, W. and Belhomme, B. (2011 apr). Automated high resolution measurement of heliostat slope errors. *Sol. Energy*, vol. 85, no. 4, pp. 681–687. ISSN 0038092X.
Available at: `http://linkinghub.elsevier.com/retrieve/pii/S0038092X1000023X`

Wu, Z., Gong, B., Wang, Z., Li, Z. and Zang, C. (2010). An experimental and numerical study of the gap effect on wind load on heliostat. *Renew. Energy*, vol. 35, no. 4, pp. 797–806. ISSN 09601481.
Available at: `http://dx.doi.org/10.1016/j.renene.2009.09.009`